ACKNOWLEDGMENTS

I am deeply indebted to Professor Sanford Klein for his continuous support and numerous helpful criticisms. It is a pleasure to pursue research under his guidance.

Professors Mitchell, Duffie and Beckman have also been very helpful. The graduate students and staff of the Solar Energy Laboratory have provided stimulus and comaraderie.

I could not undertake this project, or conclude it, without the love and understanding given by Orchard.

ABSTRACT

Mathematical models are formulated of three building component types that are related to the direct solar heating of buildings. First, overhang and wingwall shading components are modelled resulting in a definition of G_s, the mean solar radiation incident on a vertical shaded collector. Next, a window component with optional night insulation is modelled, giving the sum of the solar and thermal energy transferred from the environment into the building. Finally, a one-dimensional thermal circuit model of a collector-storage wall is described. The model is compared with a two-dimensional model of the collector-storage wall. A method of computing the thermocirculation air flow in the gap between the wall surface and the cover glazing is presented.

A reference building is described and its annual energy consumption is simulated on a computer using hourly meteorological data from Madison, Wisconsin. $\mathcal{F}$, the annual fraction of the reference building load met by solar energy is defined. Portions of the reference load south wall are replaced by equal areas of the collector-storage wall or window component. The system is simulated using the same meteorological data. The

TABLE OF CONTENTS

NOMENCLATURE

Not all of the symbols used in this thesis are listed here. Symbols used locally are defined where they appear.

A - collector area

A_g - gap cross-section area

A_i - collector area irradiated by direct beam

A_s - collector area shaded from direct beam

A_v - inlet (or outlet) wall vent area

b - spacing between wall surface and first cover glazing

C - building thermal capacitance

C_p - specific heat

D_H - hydraulic diameter

e_B - bottom wingwall extension

e_L - left overhang extension

e_R - right overhang extension

e_T - top wingwall extension

$\tilde{e}$ - relative overhang extension

f_i - fraction of the collector irradiated by direct beam

$\bar{f}_i$ - monthly average fraction of the collector irradiated by direct beam

F_R - collector heat removal factor

F_{c-g} - collector radiation view factor of the ground

xv

$\bar{H}_b$ — monthly average beam solar radiation on a horizontal surface

$\bar{H}_d$ — monthly average diffuse solar radiation on a horizontal surface

$\bar{H}_s$ — monthly average solar radiation per unit shaded collector area

$\bar{H}_o$ — monthly average extraterrestrial solar radiation on a horizontal surface

k — thermal conductivity of collector-storage wall

k_a — thermal conductivity of air

$\bar{K}_T$ — atmospheric clearness index (ratio of $\bar{H}$ to $\bar{H}_o$)

KL — product of the extinction coefficient and the thickness of one cover glazing

m_i — mass of collector-storage wall node i per unit area

$\dot{m}$ — mass flow rate

nc — number of cover glazings

N — number of nodes in collector-storage wall model

p — projection of shading component

$\tilde{p}$ — relative overhang projection

Pr — Prandtl number

$\dot{q}$ — rate of energy transfer per unit area

$\dot{q}_b$ — rate energy is transferred from back of collector-storage wall to building per unit area

$\dot{q}_\ell$ — rate that collector-storage wall transfers energy through covers to environment per unit area

$\dot{q}_s$ — rate solar energy is transmitted through window or absorbed by wall per unit area

R_b — ratio of incident beam radiation on the collector surface to incident beam radiation on the horizontal surface

$\bar{R}_b$ — total beam radiation on a collector surface in a month divided by the total beam radiation on a horizontal surface in the same month

Re — Reynolds number

RI — refractive index of the glazing

R_{NI} — thermal resistance of night insulation

t — time

T — temperature

T_a — ambient air temperature

T_b — building temperature

T_g — temperature of the inside cover of the collector-storage wall

T_i — temperature of collector-storage wall node i

T_{in} — gap inlet air temperature

T_m — mean air temperature in the gap

T_N — temperature of inside surface of the collector-storage wall

T_o — gap outlet air temperature

T_1 — collector-storage wall outside surface temperature

U_b — energy transfer coefficient between collector-storage wall inside surface and building

U_L — flat plate collector overall energy loss coefficient

U_t — collector-storage wall top loss coefficient

$(\tau\alpha)_b$ – transmittance-absorptance product for beam radiation

$(\tau\alpha)_d$ – transmittance-absorptance produce for diffuse and ground reflected radiation

ϕ – latitude

ψ – profile angle

ω – hour angle

Ω – maximum profile angle for the collector to remain shaded

CHAPTER 1

INTRODUCTION

1.1 Objectives

Historically, windows were openings in building walls that allowed sunlight and fresh air to enter the building. The window opening could be closed with shutters to protect the interior from harsh weather. The use of glass over the opening transmitted sunlight into the building and permitted a view out of the building while separating the interior and exterior environments. The energy costs of glass and the prevailing masonry and timber construction techniques prevented the use of glass on more than small fractions of the building facade. The exploitation of easily recoverable fossil fuels changed the emphasis in building design from labor intensive materials to energy intensive materials. Steel structures with glass skins have become the symbol of modern architectural excellence. Buildings are shut off from the environment, and the relationship between the building and sun is often ignored. Mechanical cooling systems are required to remove internal and solar heat gains. Presently, the realization that fossil fuels are and always have been finite has precipitated a reevaluation of building design and the function of

Few climates are as ideal for solar energy utilization as the southwest United States. To provide a useful solar gain during winter in most climates, a massive wall must be covered with a transparent glazing to reduce the energy lost to the environment. Where the winter climates are very cold, insulation must be placed between the wall and environment at night to keep energy losses from overcoming the gains. Building components including thermal storage walls and cover glazings are referred to as collector-storage walls.

It is necessary to shade windows and collector-storage walls during summer to prevent excessive solar heat gains. Fortunately the sun changes its position between winter and summer. During winter, when solar energy gains are desired, the altitude of the sun is low and the sun is to the south (north in the Southern hemisphere) of the building. Generally the south wall is the most appropriate building surface to use as a solar collector. During summer, when solar gains are not desired, the altitude of the sun is high. A building component, such as an overhang, can be placed to shade the collector from the sun during the summer but not during the winter.

mathematical model of the system and simulate the system performance on a computer using hourly measured meteorological data to drive the simulation. Model parameters can be varied and the simulation repeated. The effect of design parameters on system performance can then be measured. TRNSYS Version 10.1 (developed by the Solar Energy Laboratory, University of Wisconsin-Madison) is a transient system simulation program. It is used in this study to simulate the performance of buildings directly heated by solar energy.

When solar collectors such as windows are directly coupled with the building, it is necessary to shade the collectors during summer to prevent overheating. The shading component will reduce the solar radiation incident on the solar collector throughout the year. As the performance of the solar collector is dependent on the solar energy it receives, a method of estimating the long term average daily solar radiation on the shaded collector surface would be useful. A method to estimate long term radiation on unshaded surfaces is presented by Klein (1977). That method is extended in this study to include shaded, vertical surfaces.

thermal resistance of the insulation.

In chapter 4 a model of the collector-storage wall is presented. A one-dimensional thermal circuit network is used to model the wall. As energy flow through the wall is two-dimensional, one and two dimensional models are compared. A method of calculating the mean gap air velocity when the air flow is driven by buoyant forces is given.

In chapter 5 a building to be simulated with the collector and shading components is described. Base loads without solar components are simulated.

In chapter 6 the effect of varying collector-storage wall design parameters is studied. The annual solar fraction, $\mathscr{F}$, is defined and then used to measure the performance of the solar system. The design parameters varied are the collector area, number of covers, night insulation, wall thickness, wall thermal conductivity, wall thermal capacitance, air mass flow rate through the gap and overhang design.

In chapter 7 the effect on the solar fraction of varying direct gain system parameters is studied. Parameters varied are the collector area, number of covers, building thermal capacitance, thermal resistance of the night insulation, and summer cooling strategies. Direct gain systems are compared with collector-

(Olgyay and Olgyay, 1957). Methods of designing build-
ing components and of locating trees to shade buildings
during summer are presented. Examples of many build-
ings showing a wide variety of shading devices are pre-
sented. Design With Climate (Olgyay, 1962) expanded the
earlier work to include human response to temperature,
radiation and humidity, evaluation of climate, effect
of building design on wind induced ventilation, and the
thermal effects of materials.

Direct gain and collector-storage wall systems have
been simulated at Los Alamos Scientific Laboratory.
Papers detailing the studies are referred to in the
text as they relate to the simulations analyzed in this
text. The Los Alamos studies have resulted in the
development of design methods for direct gain systems
(Wray, Balcomb, and McFarland, 1979) and collector-
storage wall systems (Balcomb and McFarland, 1978). These
methods are empirical correlations and are restricted
to the values of the parameters specified.

Jones (1979) has developed a method of estimating
the long term solar radiation on vertical collectors
shaded by overhangs for any collector azimuth. The
method is analytical but limited to the assumption that
the overhang extends infinitely past both sides of the

CHAPTER 2
OVERHANG AND WINGWALL SHADING COMPONENT MODEL

2.1 General Description

When a building component is designed to be a solar collector admitting incident winter solar radiation, it becomes necessary to shade the solar collector during summer. This chapter describes the modelling of an overhang and/or wingwalls designed to shade vertical solar collectors. An overhang is a building element projecting outward horizontally from the building wall. The overhang is located above the solar collector. A wingwall is a building element projecting outward vertically from the building wall and located to the left and/or right of the solar collector. (Left and right are defined from the point of view of an observer outside the building.) Overhangs are appropriate shading devices when collectors face south. Wingwalls are appropriate shading devices when collectors face east or west. As it is generally advantageous to orient collectors toward the south, the overhang is a more useful shading device. The emphasis in the following analysis is placed on the overhang.

2.2 Geometry of Vertical, Shaded Solar Collectors

The geometry of a vertical solar collector shaded
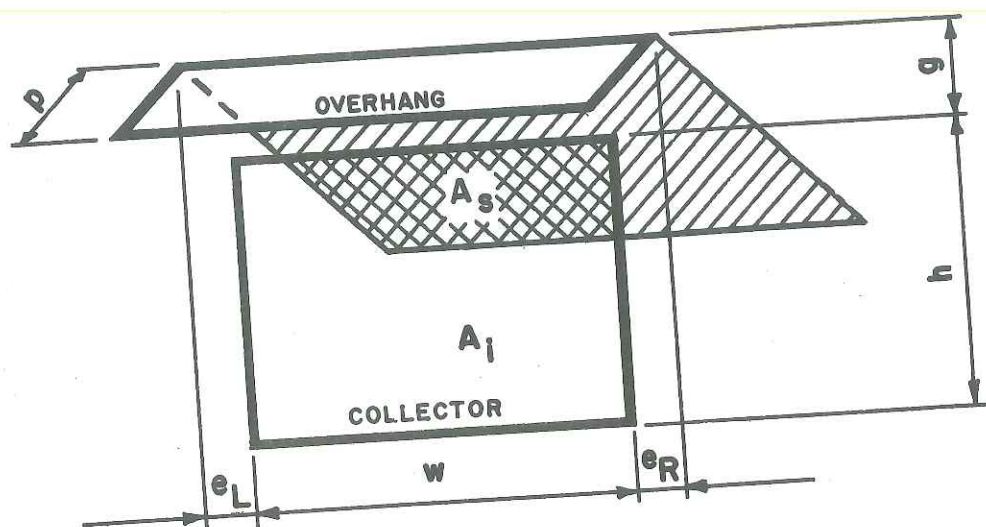
(a) COLLECTOR SHADED BY OVERHANG
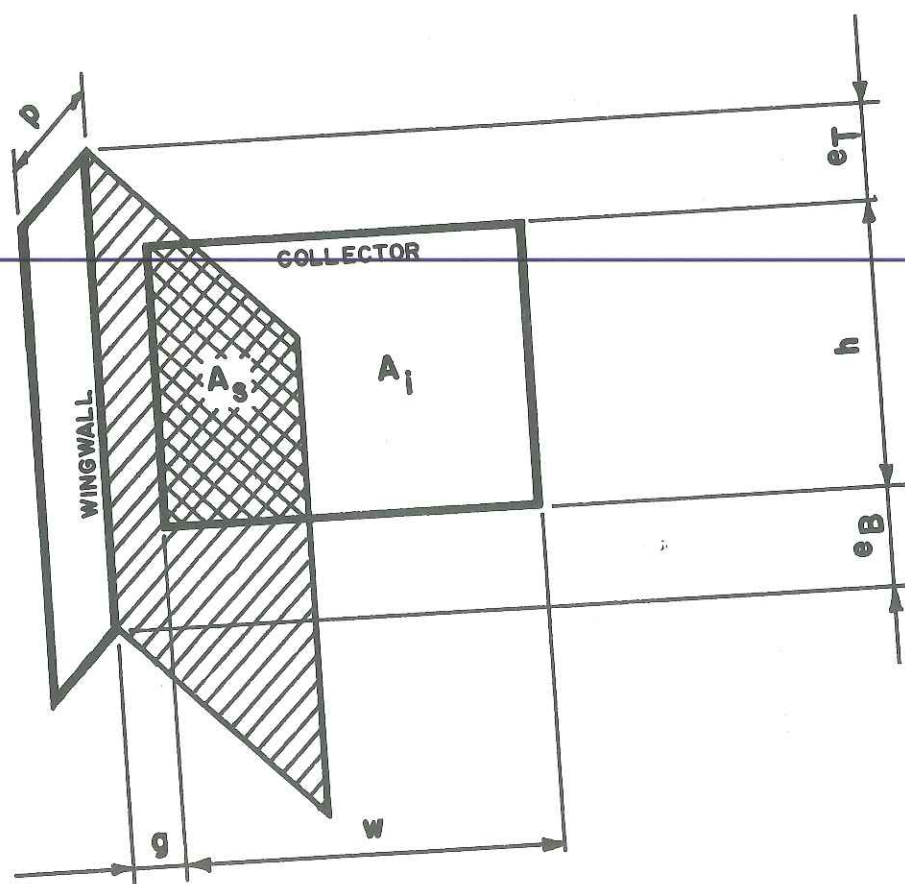
(b) COLLECTOR SHADED BY WINGWALL

Figure 2.1 Geometry of Vertical Shaded Solar Collectors

Figure 2.2   Location of the Shadow on a Shaded Collector

tal surface. ρ is the ground reflectance. F_{c-s} and F_{c-g} are the collector radiation view factors of the sky and ground. The derivation of F_{c-s} and F_{c-g} are given below. Combining equations [2.1] and [2.6] gives

$$G_s = G_b R_b f_i + G_d F_{c-s} + \rho G F_{c-g} \qquad [2.7]$$

2.4 Collector Radiation View Factors of the Sky and Ground

Sky and ground radiation view factors are calculated assuming diffuse and ground reflected radiation to be isotropic. For unshaded vertical collectors, F_{c-s} and F_{c-g} are equal to one half. These view factors are reduced when a shading device (i.e., an overhang and/or wingwalls) is present. The radiation geometry for a collector and overhang and a collector and wingwall are shown in Figure 2.3(a) & (b). The collector radiation view factor of the overhang, F_{c-o}, is computed by integrating the differential collector area radiation view factor of the overhang over the collector area. Referring to Figure 2.3(a), F_{c-o} is given by

$$F_{c-o} = \int_A F_{dA-A_1} \, dA + \int_A F_{dA-A_2} \, dA \qquad [2.8]$$

Where F_{dA-A_1} and F_{dA-A_2} are given by Siegel and Howell (1972)

$$F_{dA-A_i} = \frac{1}{2\pi} \left[\tan^{-1}\left(\frac{B_i}{C}\right) - \left\{ \frac{\frac{C}{B_i}}{\sqrt{\left(\frac{P}{B_i}\right)^2 + \left(\frac{C}{B_i}\right)^2}} \right\} \tan^{-1} \right.$$

$$\left. \left\{ \frac{1}{\sqrt{\left(\frac{P}{B_i}\right)^2 + \left(\frac{C}{B_i}\right)^2}} \right\} \right] \quad i = 1,2 \qquad [2.9]$$

Referring to Figure 2.3(b), F_{c-w}, the collector radiation view factor of the wingwall, is given by

$$F_{c-w} = \int_A F_{dA-A_1}\, dA + \int_A F_{dA-A_2}\, dA \qquad [2.10]$$

The overhang reduces the collector radiation view factor of the sky. However, the wingwalls reduce both the sky and the ground view factors. Assuming the ground to be an infinite plane, the collector view factors of the wingwall are apportioned to F_{c-s} and F_{c-g} according to Figure 2.3(b). $\int_A F_{dA-A_1}\, dA$ is deducted from F_{c-s} and $\int_A F_{dA-A_2}\, dA$ is deducted from F_{c-g}.

$$F_{c-s} = \frac{1}{2} - F_{c-o} - \int_A F^L_{dA-A_1}\, dA - \int_A F^R_{dA-A_1}\, dA \qquad [2.11]$$

$$F_{c-g} = \frac{1}{2} - \int_A F^L_{dA-A_2}\, dA - \int_A F^R_{dA-A_2}\, dA \qquad [2.12]$$

The superscripts L and R refer to the left and right wingwall. Equations [2.8], [2.10], [2.11] and [2.12] are solved by numerical integration.

overhang), G_{ov} would equal 3.92 percent of G. Since solar radiation on a vertical surface in winter is roughly twice as large a solar radiation on a horizontal surface (at middle latitudes), the effect of including G_{ov} in the calculation of G_s is to increase G_s by 2 percent under ideal conditions. Therefore, G_{ov} has been judged to be negligible relative to G_s and has not been included in the calculation of G_s.

A wingwall can reflect beam and diffuse solar radiation onto a collector as well as ground reflected solar radiation. However, a wingwall with a high solar reflectance will reflect unwanted summer solar radiation onto the collector as well as desired winter solar radiation. Except in northern climates where summer overheating does not pose a problem, a wingwall should be designed with a low solar reflectance. G_w, the solar radiation from the wingwall onto the collector, is given by

$$G_w = \rho_w \, F_{c-w} \, (G_b R_b f_i + G_d F_{w-s} + \rho G F_{w-g}) \qquad [2.14]$$

ρ_w is the solar reflectance of the wingwall. The term in parenthesis represents the solar radiation incident on the wingwall. Depending on the time of day, the solar radiation incident on the wingwall can exceed the solar radiation incident on the collector. Assuming a reasonable value of ρ_w to be 0.25, the significance of G_w de-

overhang projection is 2.5 ft (0.76 m) and the gap is
1.0 ft (0.30 m). The daily and seasonal variation of f_i
for two collector azimuths are presented in Figure 2.4.
The solid plots represent overhang extensions equal to
zero, and the dashed plots represent overhang exten-
sions equal to 3.0 ft (0.91 m). First, consider the
south facing wall. On the winter solstice, f_i is very
nearly one throughout the day and the extension does not
have any effect on the value of f_i. On the equinox,
f_i varies from one to 0.75. The larger extension drops
the value of f_i to 0.75 early in the day. On the summer
solstice, the sun does not rise on the collector until
the middle of the morning (the vertical segment of the
plot). With an extension of zero, f_i has a value near
0.45 at sunrise on the collector, dropping to zero near
solar noon, and increasing to 0.45 in mid afternoon at
sunset on the collector. The effect of the three foot
overhang extensions is to reduce f_i by more than fifty
percent. Ten foot extensions would reduce f_i to zero
throughout the day. An overhang with extensions can
be designed to shade a collector totally during summer
while leaving the collector unshaded during winter.
When the collector is faced 45° west of south, the
overhang is not as effective at shading the collector.

During the solstices and equinox, the overhang shades
the collector immediately after the sunrise on the
collector. As the afternoon proceeds, f_i increases
until the collector is completely unshaded from late
afternoon to sunset. The extension has little effect
in summer but does reduce f_i in the winter (when high
values of f_i are desired).

Daily and seasonal variation of f_i with wingwall
shading is shown in Figure 2.5. The collector has
the same dimensions as the collector shaded by the over-
hang. The left and right wingwalls have a projection
of 2.5 ft (0.76 m), gap of 1.0 ft (0.30 m), and top ex-
tension of 1.0 ft (0.30 m). The wingwalls shade the south facing
collector during the morning and afternoon on the solstices
and the equinox. The change of seasons has little effect
on the daily variation of f_i. When the collector faces
45° west of south, the left wingwall and right wingwall
have different effects. The right wingwall is repre-
sented by the dashed line and the left wingwall by the
solid line. The right wingwall shades the collector
more on the winter solstice than the summer solstice.
The left wingwall does not shade the collector in the
winter solstice while it does provide shading late in the
afternoon on the summer solstice. When a collector
faces east or west of south, the wingwall to the north

of the collector can provide shading during summer without shading the collector in the winter. However, the wingwall to the south of the collector is detrimental to the collector performance since it shades the collector during winter. When a collector faces south, a wingwall is not needed since an overhang can be designed to totally shade the collector during summer while leaving the collector unshaded during winter. Therefore, the remaining analysis will only consider overhangs for the shading of solar collectors.

the sun in the sky changes. Diffuse and ground reflected radiation strike the window from all directions. The transmittance of diffuse and ground reflected radiation can be computed assuming isotropic radiation. Brandemuehl and Beckman (1979) have shown that the mean angle of incidence for both diffuse and ground reflected radiation is $59.4° \pm 0.6°$ for vertical collectors.

The optical parameters required to determine the window transmittance are the refractive index, RI; the product of the extinction coefficient and the thickness of one pane, KL; and the number of covers, nc. A computer subroutine that determines the transmittance-absorptance product of a solar collector is called by the window component to compute the window transmittance.*
The solar absorptance of the building space behind the window is assumed to be one. This assumption is discussed below. Once the transmittances of beam radiation, τ_b, and diffuse and ground reflected radiation, τ_{dr}, have been computed, $\dot{q}_s$, the solar radiation transmitted into the building per unit window area is given by

$$\dot{q}_s = G_b R_b f_i \tau_b + (G_d F_{c-s} + \rho G F_{c-g})\, \tau_{dr} \qquad [3.1]$$

*See TRNSYS A Transient System Simulation Program, Version 10.1, Function Subroutine TALF.
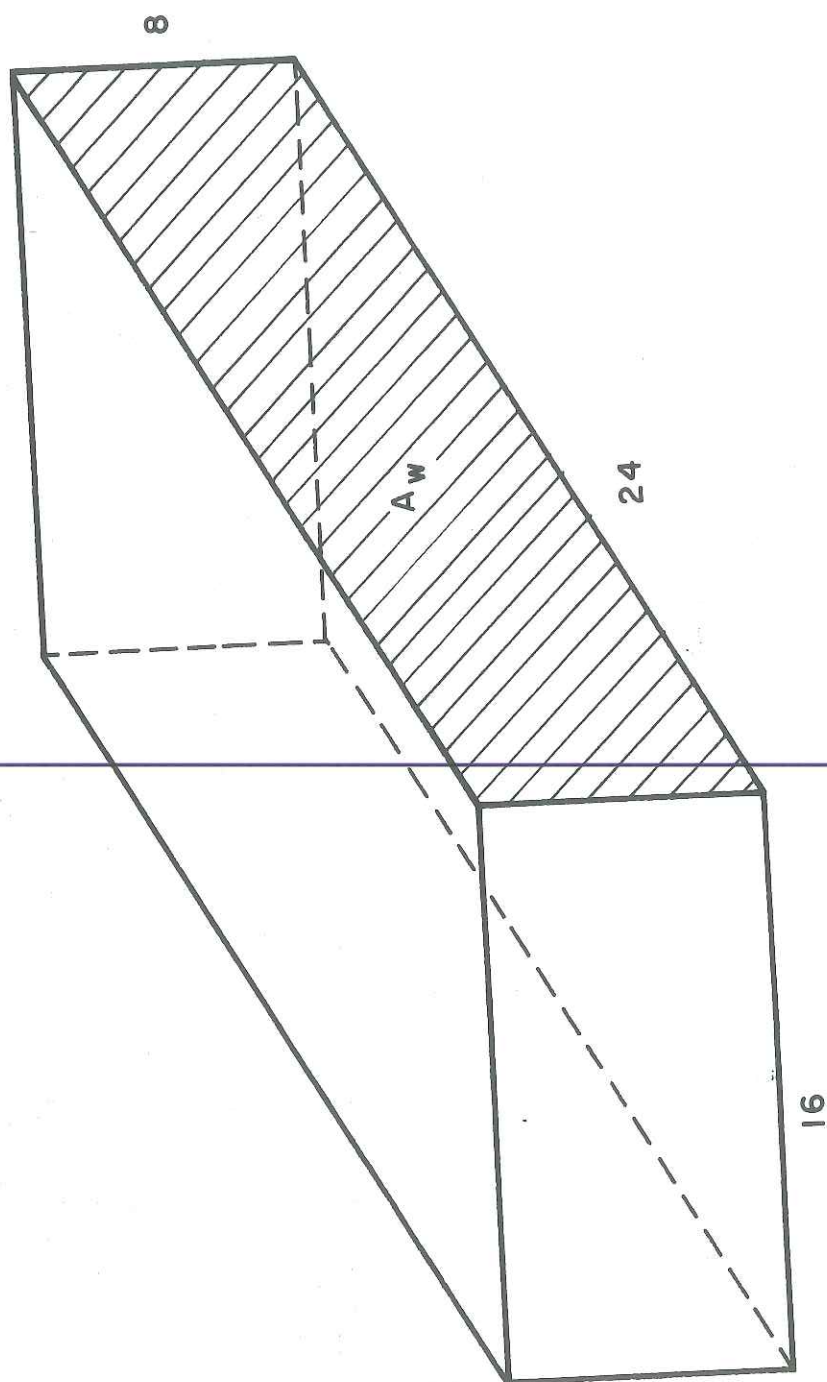
Figure 3.1 Collector and Building Dimensions for Analysis of Reflection
of Solar Energy Back Through the Collector

mainder of the analysis.

3.4 Thermal Energy Transfer Across a Window

A window, even when covered with an insulated shutter, has negligible thermal capacitance. Therefore, the thermal energy transferred across a window is modelled assuming quasi-steady state conditions. The rate at which thermal energy is transferred into the building per unit window area, $\dot{q}_t$, is given by

$$\dot{q}_t = U_w (T_a - T_b) \qquad\qquad [3.5]$$

T_a and T_b are, respectively, the ambient and building air temperatures. U_w is the heat transfer coefficient of the window assembly. In climates with moderate to severe winters, an insulated shutter could be placed over the window during the night to reduce energy losses. U_w for a window with or without night insulation can be determined from Figure 3.2. The three curves represent single, double and triple pane windows. The points on the left axis give U_w for uninsulated windows. The values are given in the ASHRAE Handbook of Fundamentals (1977)*. The figure is entered with the value of the thermal resistance of the insulating shutter and the air space be-

*Chapter 22, Table 8.

tween the shutter and window. The inside and outside air film resistances are accounted for with the uninsulated windows.

3.5 Net Energy Transferred Across a Window

The rate that energy is transferred across the window into the building, $\dot{Q}_n$, is equal to the sum of the solar and thermal energy transferred multiplied by the window area. $\dot{Q}_n$ is given by

$$\dot{Q}_n = (\dot{q}_s + \dot{q}_t)A \qquad [3.6]$$

A is the window area. Figure 3.3 presents histograms of $\dot{Q}_n/A$ for the month of January in Madison, Wisconsin. The window is a double pane glass with RI equal to 1.526 and KL equal to 0.0524. T_b equals 68^oF (20^oC) throughout the month. Figure 3.3(a) represents an uninsulated window and Figure 3.3(b) represents a window that is insulated at night with 1 inch (0.0254 m) of fiberglass at night (U_w equals 0.18 Btu/hr·ft^2·^{o}F or 1.02 w/m^2 ^{o}C when insulated). The solar gain is the same in both cases. However, the thermal losses are nearly equal to the solar gains for the uninsulated case, and roughly one half of the solar gains for the insulated case. This example illustrates the advantage of providing insulated shutters on windows in climates with moderate to severe winters.

CHAPTER 4

COLLECTOR-STORAGE WALL COMPONENT MODEL

4.1 General Description

A collector-storage wall combines solar energy collection and storage into the same unit. The wall is constructed with materials having large thermal capacities, such as concrete or containers filled with water. Solar radiation transmitted by the cover glazing is absorbed on the outside surface of the wall. A portion of the absorbed solar radiation reaches the building by either of two paths. One path is via conduction through the wall. From the inside surface of the wall, energy is convected and radiated into the building. The second path is via convection from the hot outer wall surface to air in the gap between the wall and first cover. Building air flowing through the gap is heated, carrying energy back into the building. The movement of air in the gap can be caused either by a fan or by buoyancy. In the buoyancy case, lighter, heated air rises in the gap and enters the building through outlet vents located at the top of the wall while heavier, cool building air enters the gap through inlet vents located at the bottom of the wall. Movement of air by buoyant forces will be referred to as thermocirculation.
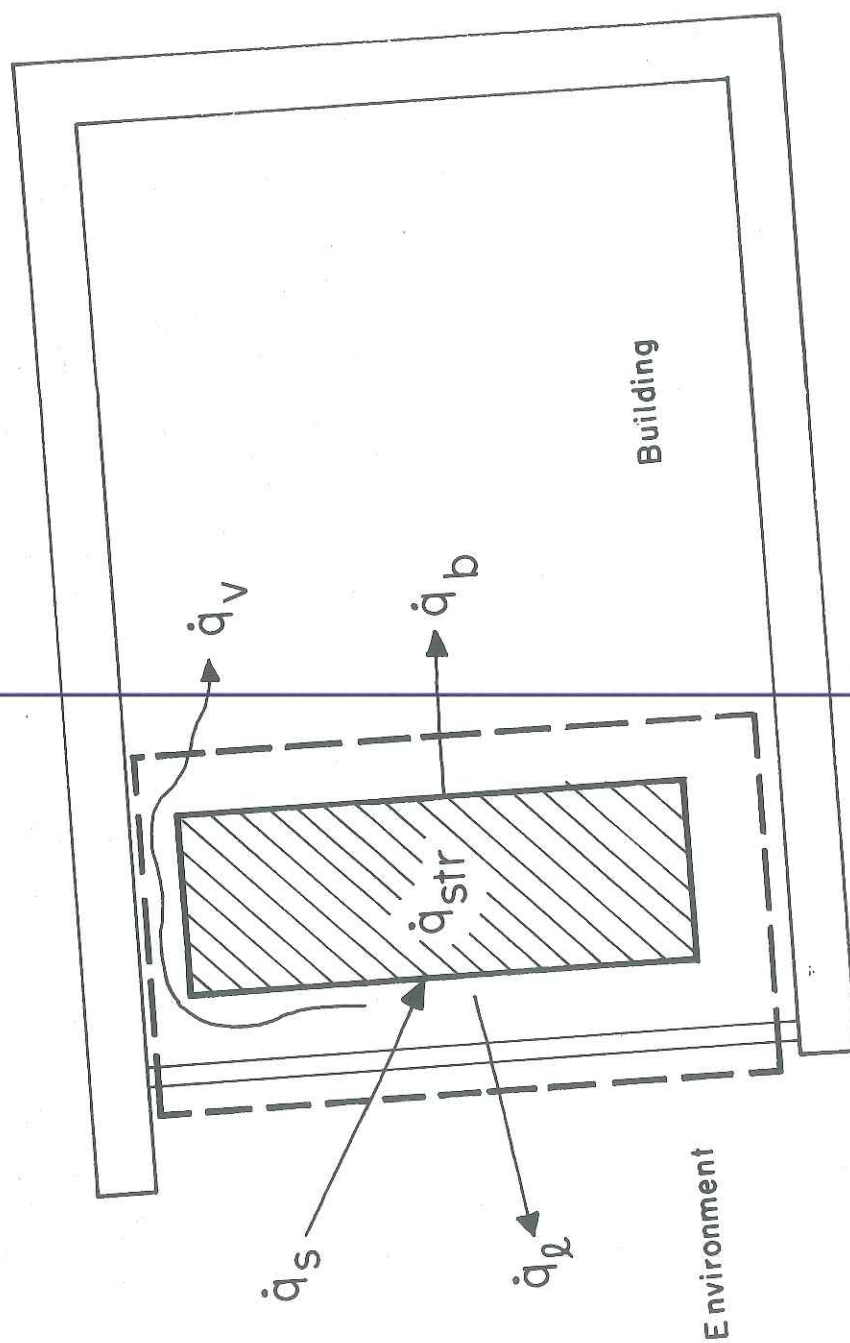
Figure 4.1   Energy Flows Through a Collector-Storage Wall
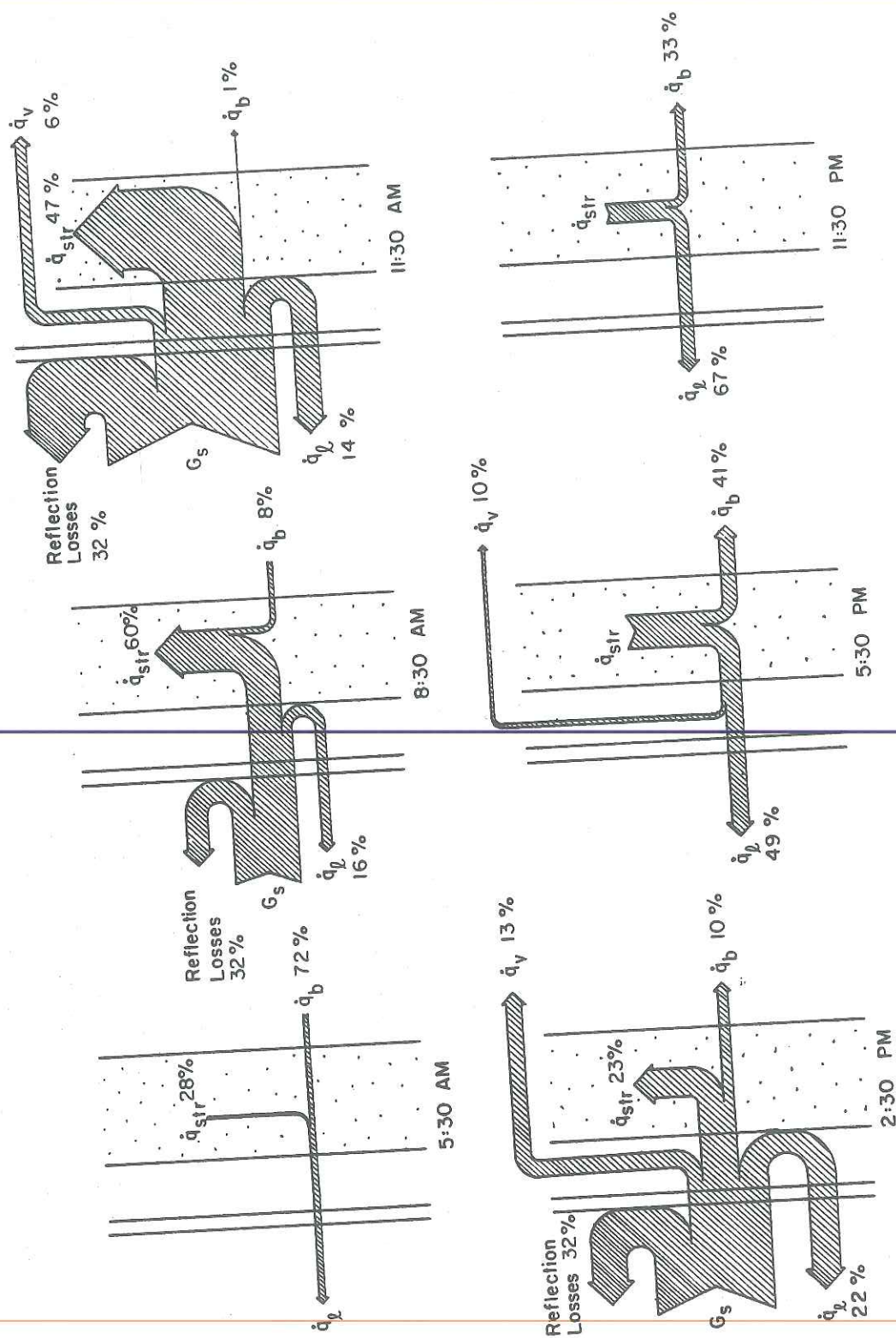
Figure 4.2 Energy Flow Through a Collector-Storage Wall During a Sunny Day

creases in losses to the environment and gains to the building. Both the losses to the environment and the building gains from heated air in the gap follow the wall surface temperature, reaching a maximum in early afternoon. Energy conducted through the wall begins to flow into the room by early afternoon, reaching a maximum early in the evening. Shortly after sunset, the wall losses equal the building gains. By midnight, the losses are twice as great as the gains. By the following morning (Figure 4.3) more than 80% of the energy being discharged by the wall is lost to the environment.

Figure 4.3 shows the energy flows through the wall on a cloudy day following the sunny day. Only during midday is the absorbed solar radiation large enough to overcome losses and charge the wall. However, much of the stored energy is lost to the environment with little reaching the building. Shortly after sundown, more than 90% of the energy discharged is lost to the environment. Some conclusions can be drawn from this analysis. First, collector-storage walls do not perform well on cold, cloudy days. (The average ambient temperatures for the two days were 16°F (-9°C) and 21°F (-5°C) respectively.) Second, since the wall loses energy 24 hours per day (as compared to an active collector), the strategy for controlling the losses will have a strong effect on the per-
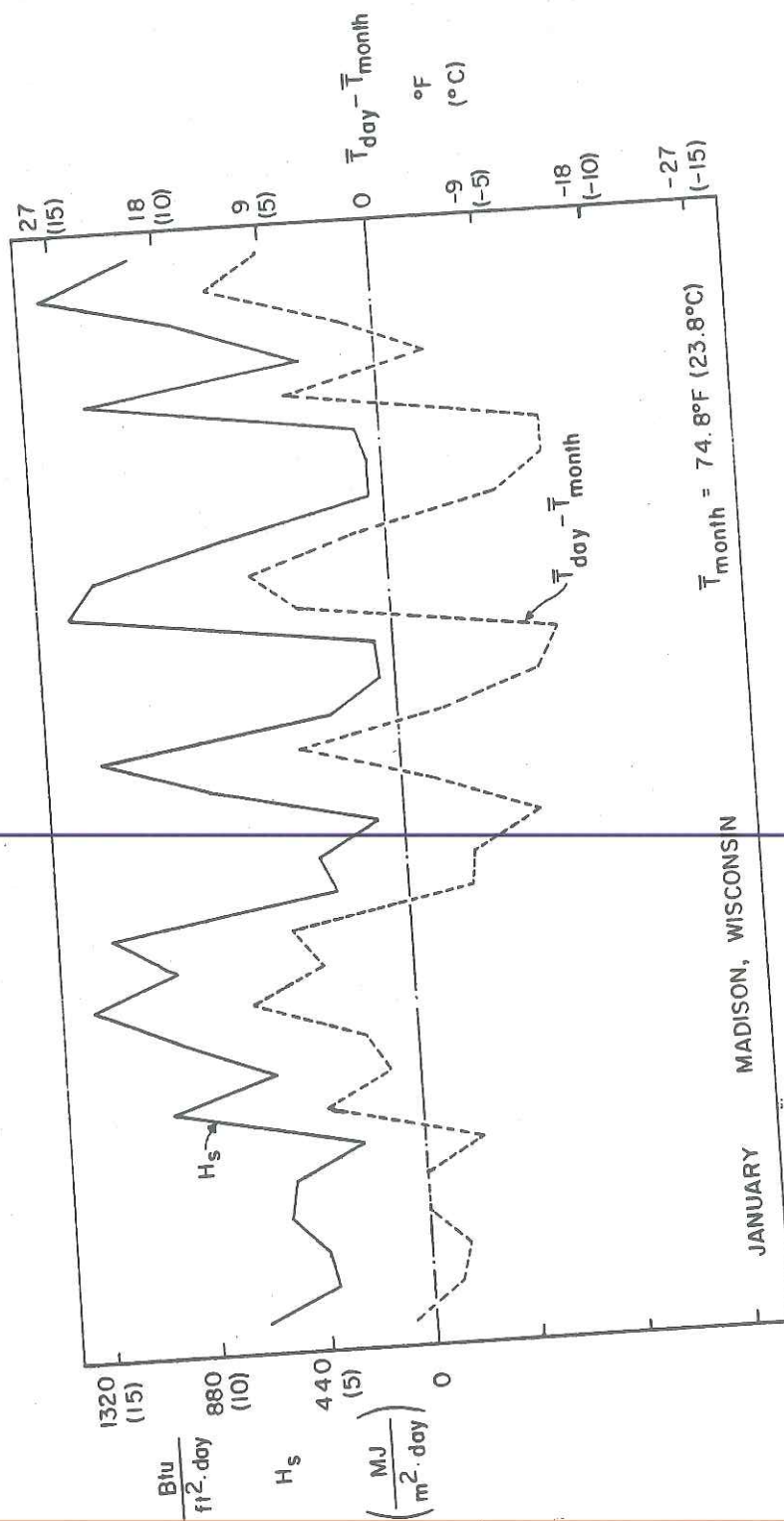
Figure 4.4   Change in Average Daily Collector-Storage Wall Temperature
as Driven by Daily Absorbed Solar Radiation

thermal capacitance. The two surface nodes have half the thermal capacitance of the interior nodes. The wall temperatures and energy flows are driven by the conditions outside the model boundary. These are the incident solar radiation, G_s; the building and environment temperatures, T_b and T_a; and the value of the control function γ. Each of the terms of equation [4.1] are computed as follows

$$\dot{q}_{str} \cong \sum_{i=1}^{N} m_i C_p \frac{dT_i}{dt} \tag{4.3}$$

$$\dot{q}_s = \begin{array}{c} (\overline{\tau\alpha})\ G_s \\ \text{or} \\ G_b R_b f_i (\tau\alpha)_b + (G_d F_{c-s} + \rho G F_{c-g})(\tau\alpha)_{dr} \end{array} \begin{array}{c} [4.4] \\ \\ [4.5] \end{array}$$

$$\dot{q}_\ell = U_t (T_g - T_a) \tag{4.6}$$

$$\dot{q}_b = U_b (T_N - T_b) \tag{4.7}$$

$$\dot{q}_v = \frac{\dot{m}Cp}{A} (T_o - T_{in}) \tag{4.8}$$

The terms on the right side of equations [4.3] through [4.8] are described below.

The change in energy stored in the wall per unit area, as approximated by equation [4.3], is equal to the sum of the change in energy stored in each element of

The superscript $^-$ refers to temperatures from the previous timestep. A modified Euler method is used to solve the differential equations. The network model is subject to instabilities if the timestep chosen is too large. The critical timestep for the component model, Δt_c, is given by

$$\Delta t_c = \frac{\rho C_p \Delta x}{2} \left\{ MIN \left[\frac{1}{h_r + h_c + \frac{k}{\Delta x}} , \frac{1}{U_b + \frac{k}{\Delta x}} \right] \right\} \qquad [4.14]$$

The dynamics of the total simulation may require a time-step smaller than Δt_c. h_r is the effective radiation heat transfer coefficient between the outer wall surface and the first cover. h_c is the convection heat transfer coefficient between the outer wall surface and the air in the gap. U_b is the combined radiation and convection heat transfer coefficient between the inside wall surface and the building. k is the thermal conductivity of the wall.

The solar energy absorbed by the wall, $\dot{q}_s$, is determined in the manner described in Chapter 3, section 3.2, except, α_w the solar absorptance of the wall is included. (In Chapter 3 it was assumed that the solar absorptance of the building was equal to one.)

The collector-storage wall energy loss through the glazing, $\dot{q}_\ell$, can be determined by two methods depending

U_b is the combined radiation and convection heat trans-
fer coefficient. It is an input to the component. Under
normal conditions the value of U_b would be 1.0 to 1.5
$\frac{Btu}{Hr \ ft^2 \ ^oF}$ [5.7 to 8.5 $\frac{w}{m^2 \ ^oC}$]. In this study, U_b is
equal to 1.5 Btu/hr ft^2 ^oF (8.5 w/m^2 ^oC).

The energy carried by air flowing through the gap
to the building (or to the environment) is given by
equation [4.8]. $\dot{m}$ is the mass flow rate of air in the
gap. For forced convection $\dot{m}$ is an input to the compon-
ent. For thermocirculation $\dot{m}$ is driven by buoyant forces
and the value of $\dot{m}$ is determined internally. The model-
ing of thermocirculation flow is described in section
4.4. C_p is the specific heat of the air. T_{in} is the
inlet air temperature. If γ equals 1, T_{in} equals T_b.
If γ equals -1, T_{in} equals T_a. T_o is the outlet temper-
ature of the air. T_o can be determined from an energy
balance on a differential volume of air in the gap per-
pindicular to the flow. The energy balance yields (see
Figure 4.6).

$$\dot{m} \ C_p \ \frac{dT}{dz} = h_c \bar{w} \ (T_1 - T) + h_c w \ (T_g - T) \qquad [4.18]$$

T is the air temperature in the gap at position z. w is
the width of the wall. Separating the variables and
integrating equation [4.18] over the flow length L and
solving the result for $(T_o - T_{in})$ yields

$$T_o - T_{in} = \frac{2T_{in} - T_1 - T_g}{2} \left[\text{EXP} - \left\{ \frac{2h_c A}{\dot{m}C_p} \right\} - 1 \right] \qquad [4.19]$$

However, in the one-dimensional model, $\dot{q}_v$ is determined from T_m, the mean air temperature in the gap, and the resistance to energy transfer through air flow in the gap. T_m is defined by

$$T_m - T_{in} = \frac{1}{L} \int_o^L (T - T_{in}) \, dz \qquad [4.20]$$

where

$$T - T_{in} = \frac{2T_{in} - T_1 - T_g}{2} \left[\text{EXP} - \left\{ \frac{2h_c wz}{\dot{m}C_p} \right\} - 1 \right] \qquad [4.21]$$

Inserting equation [4.21] into equation [4.20] and performing the integration yields

$$T_m - T_{in} = \frac{2T_{in} - T_1 - T_g}{2} \left[-\frac{\dot{m}C_p}{2h_c A} \left(\text{EXP} - \left\{ \frac{2h_c A}{\dot{m}C_p} \right\} - 1 \right) - 1 \right] \qquad [4.22]$$

The resistance to energy transfer through the air stream per unit area, R, is defined by

$$R = \frac{\Delta T}{\dot{q}_v} = \frac{A(T_m - T_{in})}{\dot{m}C_p(T_o - T_{in})} \qquad [4.23]$$

Combining equations [4.19], [4.22] and [4.23] yields

tion for convection heat transfer between vertical parallel plates given by Randall, et al. (1979)

$$h_c = \left[0.0965 \, (Gr \cdot Pr)^{0.29}\right] \frac{k_a}{b} \qquad [4.27]$$

k_a is the thermal conductivity of the air. b is the plate spacing. Gr is the Grashof number. Pr is the Prandtl number. When air is flowing in the gap, the value of h_c depends on whether the flow is laminar or turbulent. If the flow is laminar (Reynolds number is less than 2000), then h_c is determined from the following correlation for flow between parallel plates with one plate insulated (the glass cover approximates an insulated plate) as given by Mercer et al. (1967)

$$h_c = \left[4.9 + \frac{0.0606 \, (x^*)^{-1.2}}{1.0 + 0.0856 \, (x^*)^{-0.7}}\right] \frac{k_a}{b} \qquad [4.28]$$

where

$$x^* = \frac{L}{Re \cdot Pr \cdot D_H} \qquad [4.29]$$

Re is the Reynolds number. D_H is the hydraulic diameter of the flow channel, which is equal to four times the flow cross sectional area divided by the flow perimeter. L is the length of the flow channel. The correlation used

$$0 = h_c(T_g - T_m) + h_c(T_1 - T_m) + \frac{1}{R}(T_{in} - T_m) \qquad [4.32]$$

Solving both equations simultaneously for T_g yields

$$T_g = \frac{T_a U_t + T_{in}\dfrac{\frac{h_c}{R}}{2h_c + \frac{1}{R}} + T_1\left[h_r + \dfrac{h_c^2}{2h_c + \frac{1}{R}}\right]}{h_r + U_t + h_c + \left[\dfrac{h_c^2}{2h_c + \frac{1}{R}}\right]} \qquad [4.33]$$

T_m can then be calculated after rearranging equation [4.32]

$$T_m = \frac{\dfrac{T_{in}}{R} + (T_g + T_1)\, h_c}{2h_c + \frac{1}{R}} \qquad [4.34]$$

4.3 Comparison of One and Two-dimensional Models

An implicit assumption in the one dimensional thermal circuit model is that the wall and glass temperatures are independent of position in the flow direction during periods of air flow in the gap. In order to test this assumption, a computer simulation is set up with five collector-storage wall components connected in series. Each component is 3.28 feet (1 meter) wide, 3.28 feet (1 meter) long and 0.67 feet (0.2 meter) thick. The total length of the flow channel is 16.4 feet (5 meters).

Two – dimensional Model

One – dimensional Model
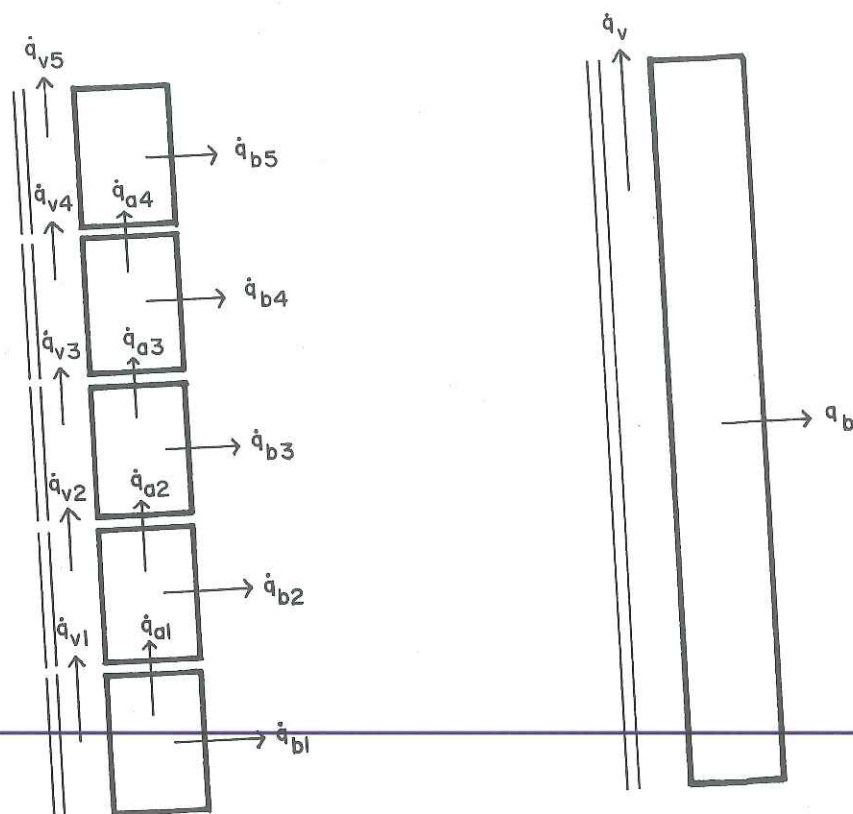
$$\dot{q}_v = \dot{q}_{v1} + \dot{q}_{v2} + \dot{q}_{v3} + \dot{q}_{v4} + \dot{q}_{v5}$$

$$\dot{q}_b = \dot{q}_{b1} + \dot{q}_{b2} + \dot{q}_{b3} + \dot{q}_{b4} + \dot{q}_{b5}$$

Figure 4.7   One and Two-dimensional Models of the
Collector-Storage Wall

Table 4.2

Comparison of One and Two Dimensional Models
with Linear and Exponential Temperature Profiles
for a mass flow rate of $110 \frac{lbm}{Hr} \left(50 \frac{kg}{Hr}\right)$
Energy Flows for October, Madison, Wisconsin

	Q_v Btu (KJ)	Q_b Btu (KJ)	Qaxial (average) Btu (KJ)
One Dimensional Models			
Exponential Profile	123400 (117000)	647800 (614000)	--
Linear Profile	126700 (120100)	646500 (612800)	--
Two Dimensional Models			
Exponential Profile	123800 (117300)	647700 (613900)	47 (50)
Linear Profile	124400 (117900)	647500 (613700)	47 (50)
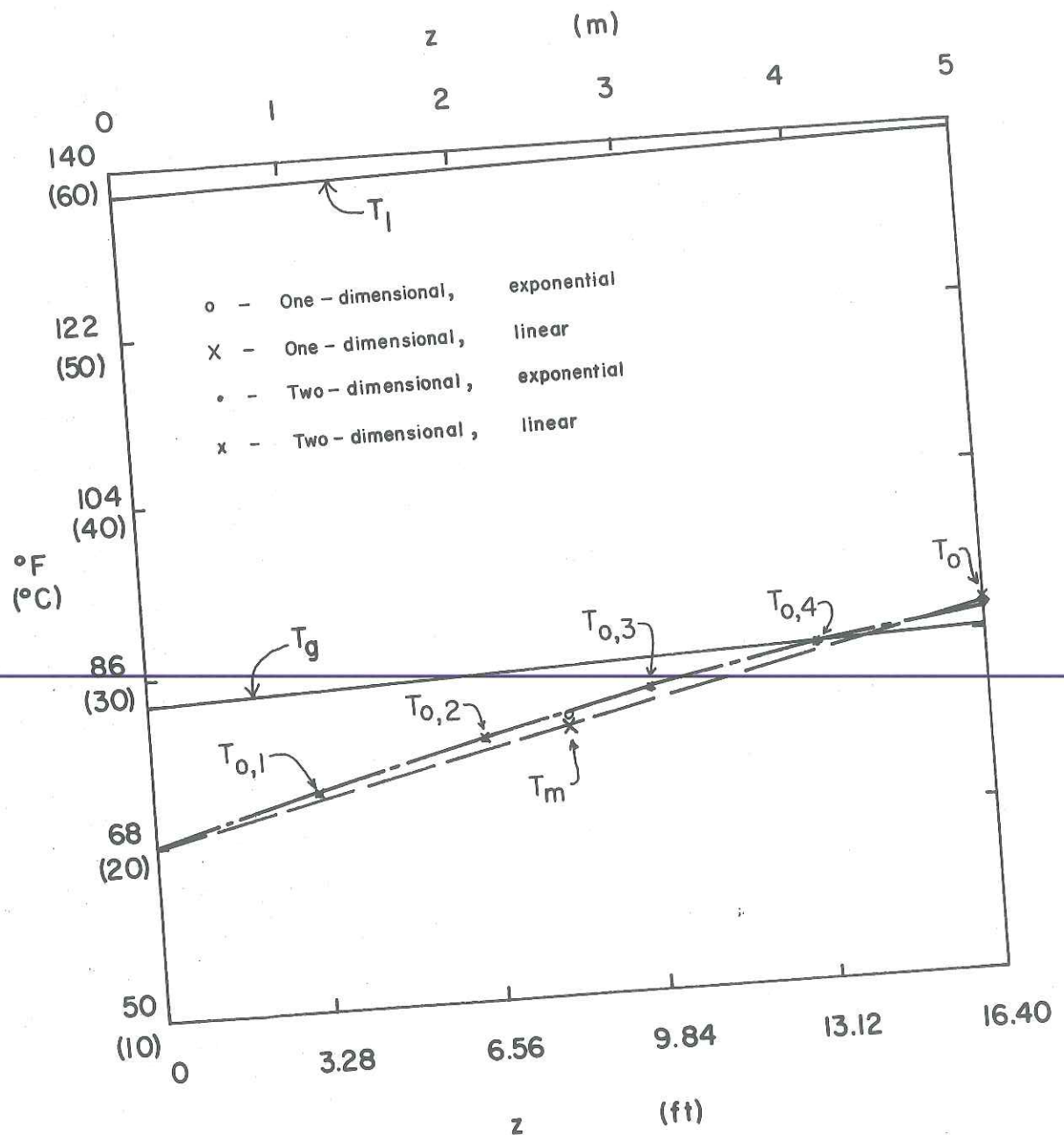
Figure 4.9 Air Temperature Profile as a Function of Position in the Gap - $\dot{m} = 110 \ \frac{lbm}{Hr} \left(50 \ \frac{kg}{Hr}\right)$

model have shown the validity of the assumptions of constant wall and glass temperature. The exponential model of the air temperature profile has also been shown to give excellent predictions of the temperature profile.

4.4 Estimating Mass Flow Due to Buoyant Forces

In the thermocirculation flow regime, air circulation through the gap is driven by density differences between the air in the gap and air in the building. The problem is to determine the pressure losses in the inlet and outlet vents and in the gap that the buoyant forces must overcome. The solution is to consider air in the building and gap to be a closed system and apply Bernoulli's equation over the entire system. Bernoulli's equation is solved for the mean air velocity in the gap. The mass flow rate can then be determined from the velocity and the gap geometry. This solution is compared to a relationship given by Balcomb et al. (1977A) using data measured by Trombe et al. (1977).

The closed system for thermocirculation air flow is shown in Figure 4.10. It is assumed that the only pressure losses in the flow occur in the inlet vent, gap, and outlet vent. For flow between points one and two, it is assumed that the air density and temperature are constant and that the air velocity at one is zero

and at two is equal to the mean air velocity in the gap, $\overline{V}g$. Bernoulli's equation, in terms of the pressure drop, is

$$P_2-P_1 = -\rho_1 \left[\hat{E}_{12} + \frac{\overline{V}g^2}{2} \right] \qquad [4.36]$$

$\hat{E}_{12}$ is the friction loss between points one and two; $\hat{E}_{12}$ will be defined below. ρ_1 is the air density at point one. Between points two and three it is assumed that the velocity is constant and that the air temperature and density vary linearly with height. The pressure drop is then given by

$$P_3-P_2 = -\overline{\rho} \; (\hat{E}_{23} + gL) \qquad [4.37]$$

$\overline{\rho}$ is the mean air density in the gap equal to the arithmatic average of ρ_1 and ρ_3. g is the acceleration of gravity and L is the vertical distance between the inlet and outlet vents. Between points three and four it is assumed that the density is constant and that the air velocity at point four is zero. The pressure drop is given by

$$P_4-P_3 = -\rho_3 \left[\hat{E}_{34} - \frac{\overline{V}g^2}{2} \right] \qquad [4.38]$$

Between points four and one it is assumed that the temperature is constant, there are no frictional losses,

tion. The square of the ratio of Ag to Av corrects $\overline{V}g^2$ to the mean vent air velocity. Inserting equations [4.41] and [4.42] into equation [4.40] and solving for $\overline{V}g$ yields

$$\overline{V}g = \sqrt{\frac{gL\,(\rho_1 - \overline{\rho})}{\overline{\rho}\left[2 + 4\left(\frac{Ag}{Av}\right)^2\right] + \overline{\rho}\left(\frac{\rho_1}{\overline{\rho}} - 1\right)}} \qquad [4.43]$$

Considering the two terms in the denominator within the square root, the following assumption is made

$$\left[2 + 4\left(\frac{Ag}{Av}\right)^2\right] >> \left(\frac{\rho_1}{\overline{\rho}} - 1\right) \qquad [4.44]$$

Equation [4.43] is rewritten

$$\overline{V}g = \sqrt{\frac{gL}{\left(2 + 4\left(\frac{Ag}{Av}\right)^2\right)} \cdot \left(\frac{\rho_1 - \overline{\rho}}{\overline{\rho}}\right)} \qquad [4.45]$$

Assuming pressure differences to be small compared to density and temperature differences, equation [4.45] can be rewritten in terms of the temperatures of the air as

$$\overline{V}g = \sqrt{\frac{gL}{\left[2 + 4\left(\frac{Ag}{Av}\right)^2\right]} \cdot \left(\frac{T_m - T_{in}}{T_{in}}\right)} \qquad [4.46]$$

and total solar energy gain, Q_u, are compared with pre-
dicted values in Figure 4.11. Measured hourly mass flow
rates are compared to predicted mass flow rates in Figure
4.12. While both models predicted Q_v fairly well, there
is a large descrepancy in the predicted and measured
values of mass flow rates. While both models predicted
higher mass flow rates, they also predicted lower sur-
face temperatures. The effects are compensating giving
similar values of Q_v. The test cannot be used to vali-
date either model. However, the comparison does show
that variations in the magnitude of the mass flow rate
(and, therefore, reasonable variations of the friction
factor) do not strongly affect the value of Q_v or of Q_u.
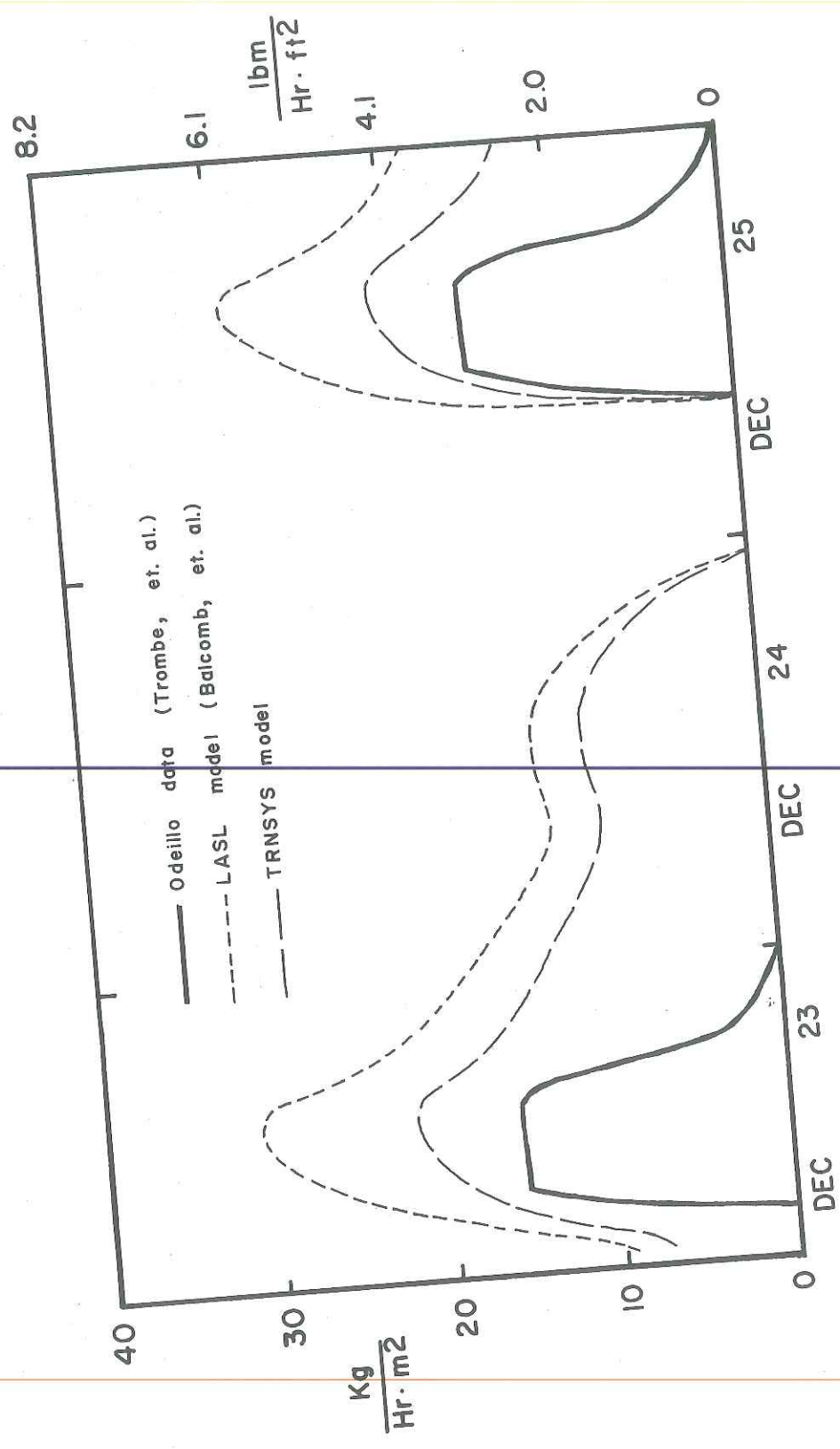
Figure 4.12 Predicted TRNSYS and LASL Mass Flow Rates Compared to Measured Odeillo Mass Flow Rates

load computations. The building skin is described in the following section. A constant air infiltration rate equal to one half the apartment unit volume per hour is used in all the simulations. Ventilation strategies are discussed in section 5.4.

The apartment air temperature is modelled with a single node using response factors built into the simulation program.* The actual apartment has rooms on the south and north sides of the building. Under most conditions during the year there is no significant temperature difference between rooms. However, experience has shown that temperature differences of up to 20°F (11°C) between south and north rooms do occur on sunny, cold winter days. Rather than model a two zone unit, it is assumed that a small fan is used to mix the air throughout the apartment.

The thermal capacitance of the apartment interior is estimated to be approximately $1 \frac{Btu}{ft^3 {}^oF}$ ($67 \frac{KJ}{m^3 {}^oC}$) or $5266 \frac{Btu}{{}^oF}$ ($10000 \frac{KJ}{{}^oC}$). The effect of varying the capacitance is discussed in chapter 7.

5.3 Description of the Building

The floor plan of the apartment unit modelled is

---

*See TRNSYS - Type 19 component description.
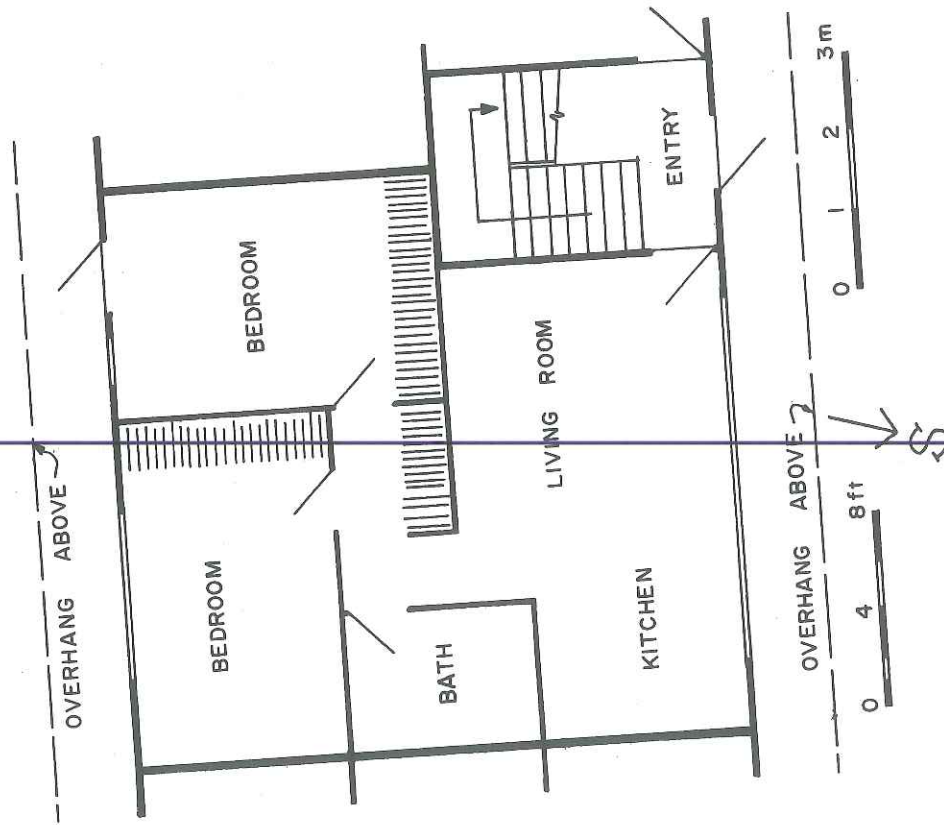
Figure 5.1 Floor Plan of a Typical Eagle Heights Apartment Unit

Table 5.1

Building Dimensions for Base Loads 1 & 2

	Base Load 1	Base Load 2
South Wall	192 ft^2 (17.8 m^2)	192 ft^2 (17.8 m^2)
window fraction	0.2	0.2
East Wall	208 ft^2 (19.3 m^2)	0
North Wall	192 ft^2 (17.8 m^2)	192 ft^2 (17.8 m^2)
window fraction	0..2	0.2
West Wall	208 ft^2 (19.3 m^2)	0
Roof	624 ft^2 (58.0 m^2)	0
UA	229 $\frac{Btu}{Hr\cdot{}^oF}$ (121 $\frac{W}{{}^oC}$)	127 $\frac{Btu}{Hr\cdot{}^oF}$ (67 $\frac{W}{{}^oC}$)

Table 5.2

Breakdown of Energy Consumption

Base Load 1

Month	Number of Hours $T_b > 80°F$ (26.7°C)	Energy Consumption MM Btu (GJ)		
		Q_{AUX}	Q_{FAN}	Q_{TOT}
January	0	8.05 (7.63)	0	8.05 (7.63)
February	0	6.82 (6.46)	0	6.82 (6.46)
March	0	5.52 (5.23)	0	5.52 (5.23)
April	0	3.13 (2.97)	0	3.13 (2.97)
May	14	0.97 (0.92)	0.03 (0.03)	1.00 (0.95)
June	152	0.04 (0.04)	0.25 (0.24)	0.29 (0.28)
July	200	0.02 (0.02)	0.30 (0.29)	0.32 (0.31)
August	41	0	0.25 (0.24)	0.25 (0.24)
September	0	0.72 (0.68)	0.06 (0.06)	0.78 (0.74)
October	0	2.00 (1.90)	0	2.00 (1.90)
November	0	4.64 (4.38)	0	4.64 (4.38)
December	0	7.03 (6.67)	0	7.03 (6.67)
Year	407	38.94 (36.90)	0.89 (0.86)	39.83 (37.76)

is the operating energy consumed by the fan used to ventilate the building. Q_{TOT} is the sum of Q_{AUX} and Q_{FAN}. Base Load 1, with losses through four walls and the roof consumes nearly twice as much energy as Base Load 2. It is important to note that the heating load is shifted toward spring and is out of phase with the solar cycle. The number of hours the room temperature exceeds $80^\circ F$ ($26.7^\circ C$) is tabulated as an indicator of the severity of overheating that may be encountered with full south walls designed to collect solar energy.

Table 6.1

Summary of Hourly Meteorological Data
Madison, Wisconsin

Month	Horizontal Solar Radiation		Degree Days		Average Temperature	
	Btu/ft² day	KJ/m² day	°F day	°C day	°F	°C
January	550	6300	1391	773	20.1	- 6.6
February	830	9400	1210	672	21.8	- 5.7
March	1190	13500	1048	582	31.2	- 0.4
April	1480	16800	655	364	43.4	6.3
May	1770	20100	284	158	46.9	8.3
June	2180	24800	58	32	71.2	21.8
July	1890	21500	22	12	72.7	22.6
August	1730	19700	61	34	68.7	20.4
September	1360	15500	243	135	58.5	14.7
October	890	10100	439	244	51.4	10.8
November	550	6300	830	461	37.3	3.0
December	460	5200	1208	671	26.0	- 3.3
Year	1240	14100	7449	4138	46.9	8.3

quired for mullions, this is equivalent to the maximum collector area for the south wall of the building.

6.2 Annual Solar Fraction

Palmiter (1979) provides a complete definition of the annual solar fraction, including system efficiencies and the value of the energy used. This analysis is limited to the energy load seen by the building with a collector-storage wall (or direct gain system in chapter 7) compared with the base energy load computed in chapter 5 (Tables 5.2 and 5.3). For this analysis the annual solar fraction is defined

$$\mathscr{F} \equiv 1 - \frac{Q_{AUX} + Q_{FAN} + Q_{PAR}}{(Q_{AUX} + Q_{FAN})_{Base\ Load}} \qquad [6.1]$$

Q_{PAR} is the parasitic power consumed by the solar collector system (i.e., power consumed by a fan used to force air through the gap in the collector-storage wall). While thermal energy consumption of a furnace and electrical energy consumption of a fan are not strictly comparable, choosing a furnace efficiency and electric conversion efficiency would limit the analysis to the type of systems chosen. $\dot{Q}_{AUX}$ and $\dot{Q}_{FAN}$ are constant hourly rates, and as such, they do give a comparative
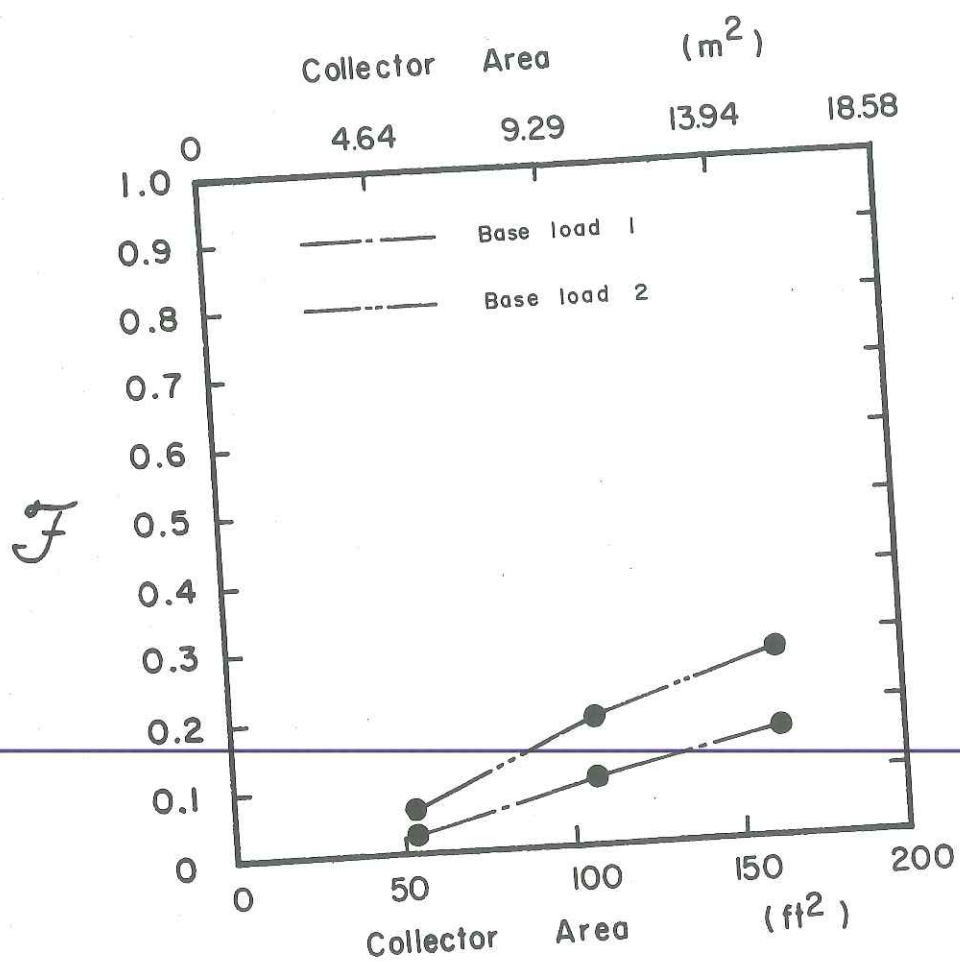
Figure 6.1   The Effect of Collector Area on the Annual
Solar Fraction - Madison, Wisconsin
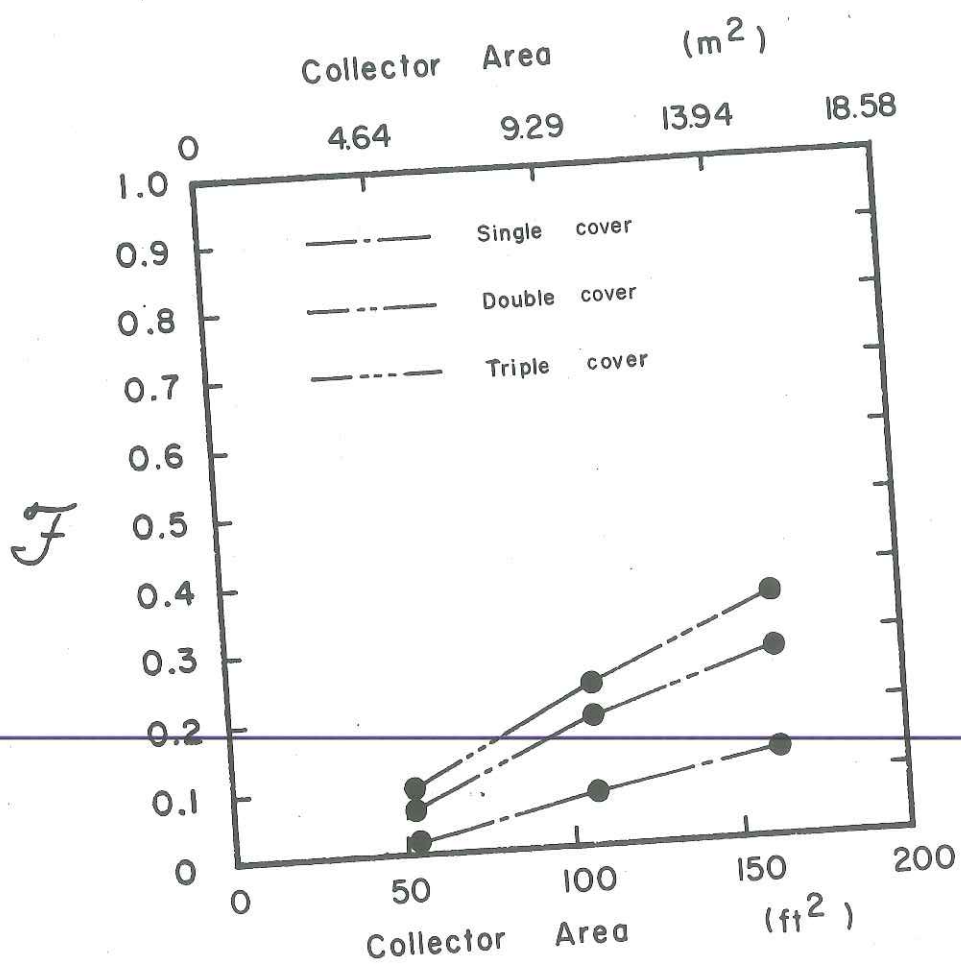
Figure 6.2   The Effect of the Number of Covers on the Annual Solar Fraction - Madison, Wisconsin
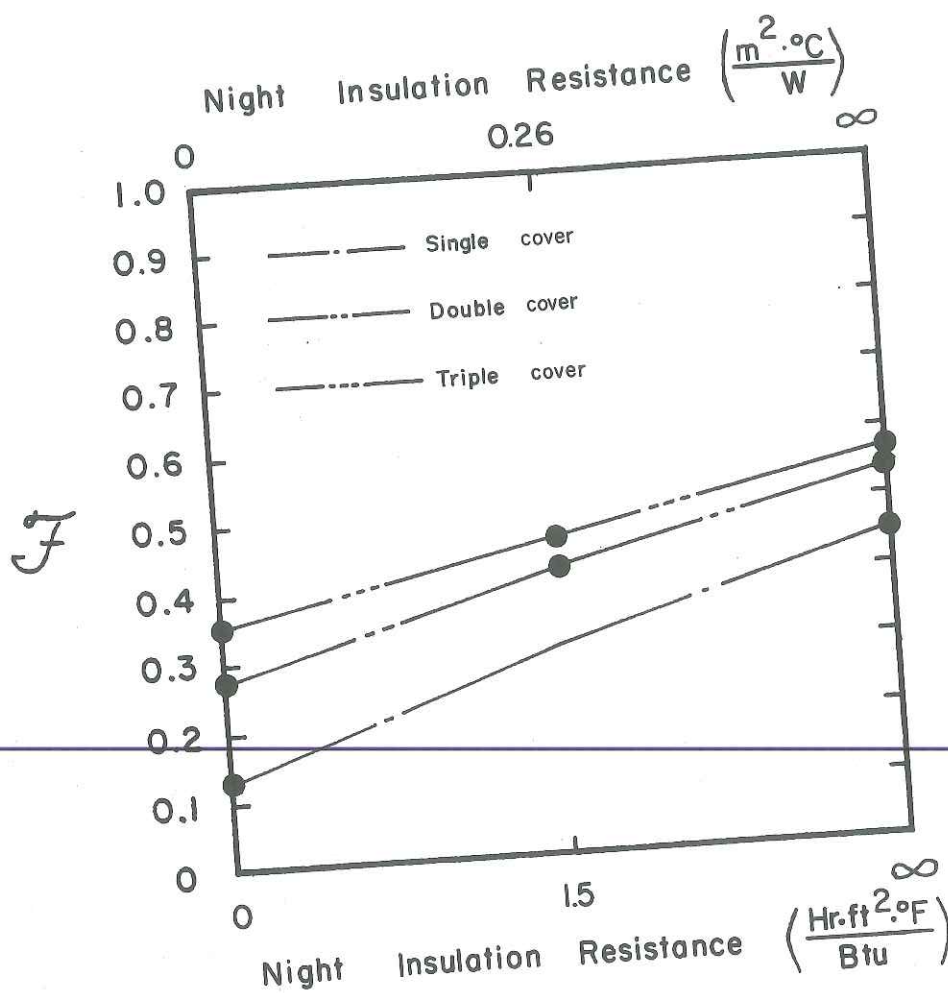
Figure 6.3 Effect of the Thermal Resistance of Night Insulation on the Annual Solar Fraction - Madison, Wisconsin

heat capacity, often referred to as the thermal capaci-
tance. Balcomb, Hedstrom and McFarland (1977B) examined
the effect of thickness and conductivity on the solar
fraction. They found that the solar fraction decreased
dramatically with decreasing thickness at high solar
fractions. Their results are in agreement with the sim-
ulation results for the Madison climate shown in Figure
6.4. The points plotted in Figure 6.4 are not related
to the same base load described in chapter 5, but are the
result of an earlier study. At high solar fractions
(i.e., collector area equal to 1000 ft^2 or 92.9 m^2),
the solar fraction decreases as the wall thickness de-
creases, in agreement with Balcomb's findings. However,
at low solar fractions (i.e., collector area equal to
100 ft^2 or 9.29 m^2) the solar fraction increases with
decreasing wall thickness. (This result was not shown in
Balcomb's study.) For a 4 in (0.1 m) wall with a
1 $\frac{Btu}{Hr\ ft\ ^oF}$ (1.73 $\frac{W}{m\ ^oC}$) thermal conductivity, the small
wall performs better than a wall ten times its size.
This surprising result can be explained with reference
to Figure 6.5, which shows the hourly rate of energy flow
from the collector storage wall to the house averaged
over the month of January for various concrete wall
thicknesses. A 4 in (0.1 m) wall transmits the daily
solar energy pulse to the house within a twelve hour
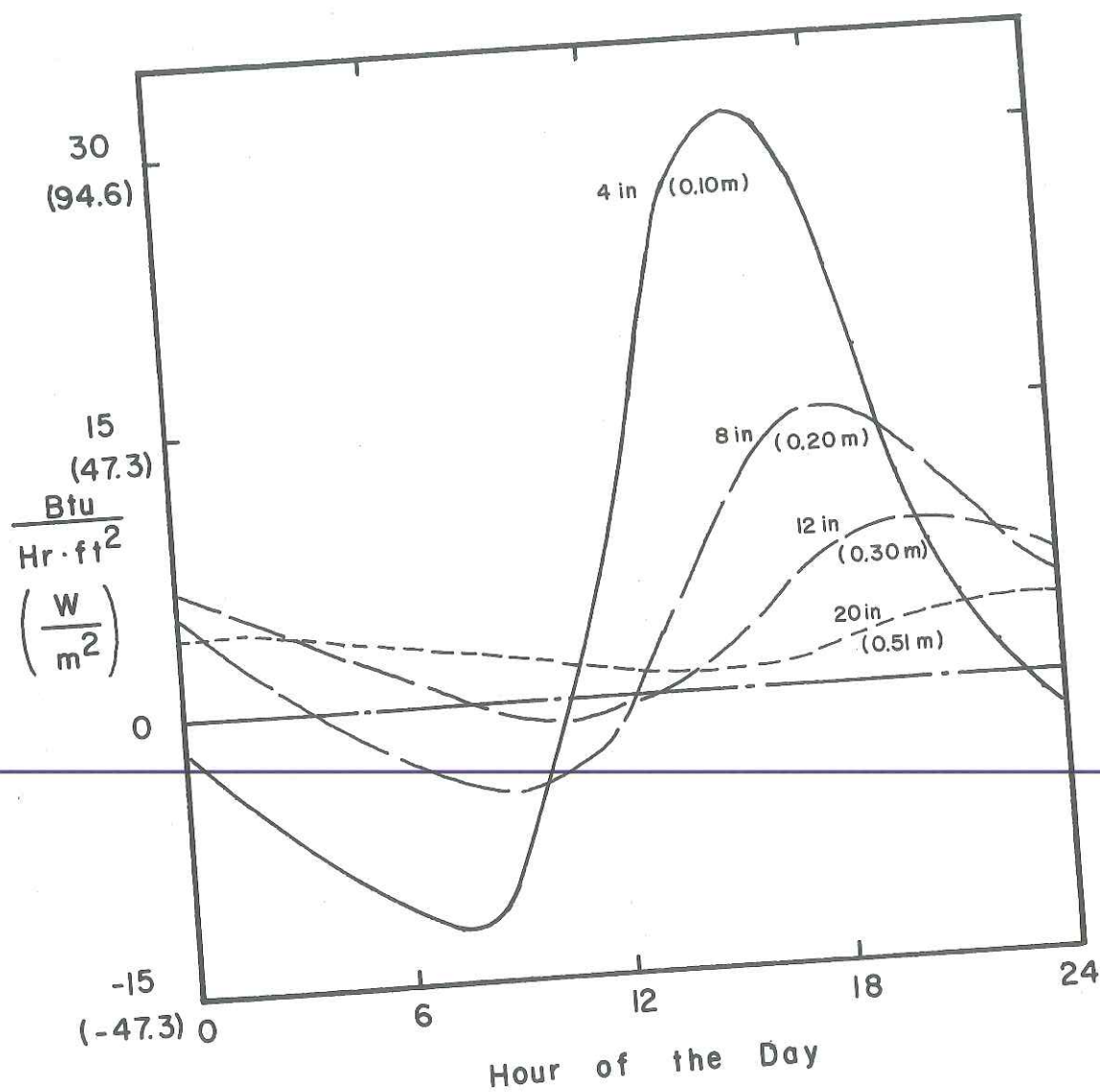
Figure 6.5 Average Rate of Energy Flow Between the Back of the Collector-Storage Wall and the Building as a Function of Wall Thickness and Time of Day - January, Madison
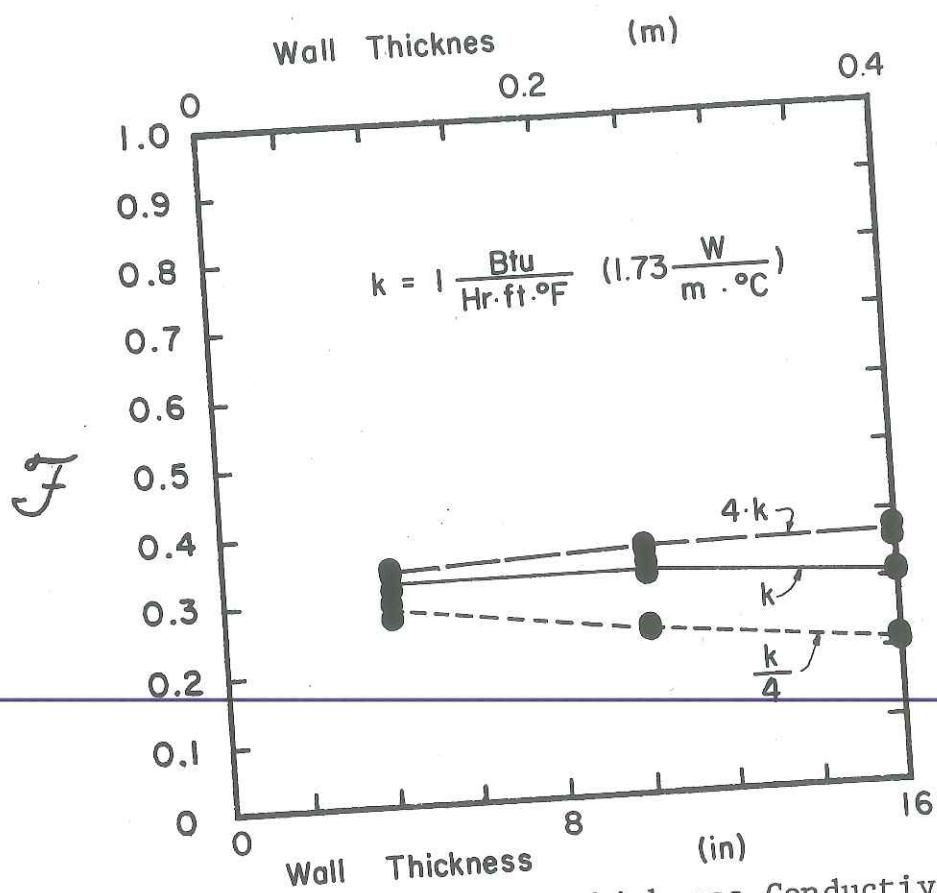
Figure 6.6 Effect of the Wall Thickness Conductivity and Thermal Capacitance on the Annual Solar Fraction - Madison, Wisconsin
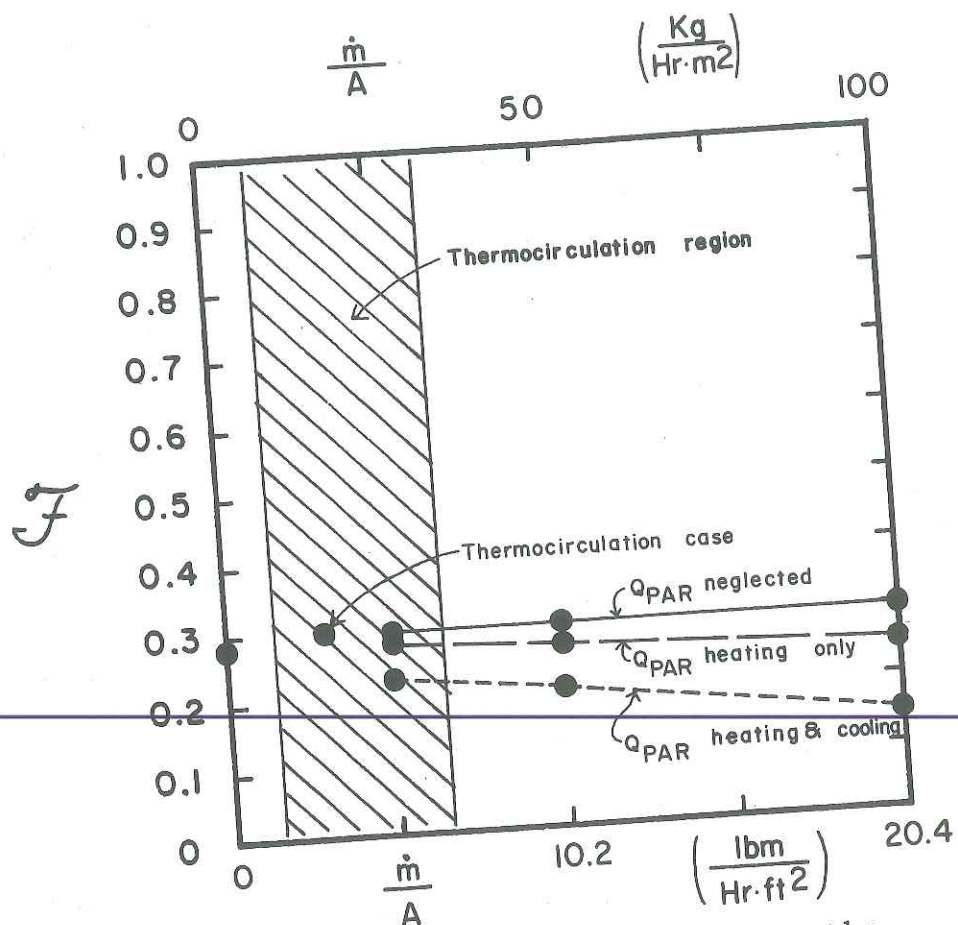
Figure 6.7 Effect of the Mass Flow Rate on the Annual Solar Fraction - Madison, Wisconsin

The fan operates approximately 150 hours per month during winter heating and 650 hours per month during summer when it is used to cool the wall. The result is a lower performance when Q_{PAR} is included for heating only and significantly lower performance when Q_{PAR} is included for heating and cooling. For Madison, Wisconsin climates, the following conclusions are drawn:

(i)   Increasing the mass flow rate does not significantly increase the solar fraction.

(ii) Using a fan to cool the wall during summer results in significant parasitic power consumption.

Ohanessian (1976) compared free and forced convection in the Australian climate and concluded that, while the distribution of solar energy gain between conduction and ventilation changed, there was no change in the total solar gain to the room. His conclusion is in agreement with conclusion (i) above. However, Sebald, et al. (1979) show a significant increase in the solar fraction when a fan is added. Sebald's model determines the top energy loss from the air in the gap to the environment rather than from the first cover. This calculation is complex in that radiation losses from the wall to the glass cover must be accounted for. This difference in model construction may have accounted for the difference
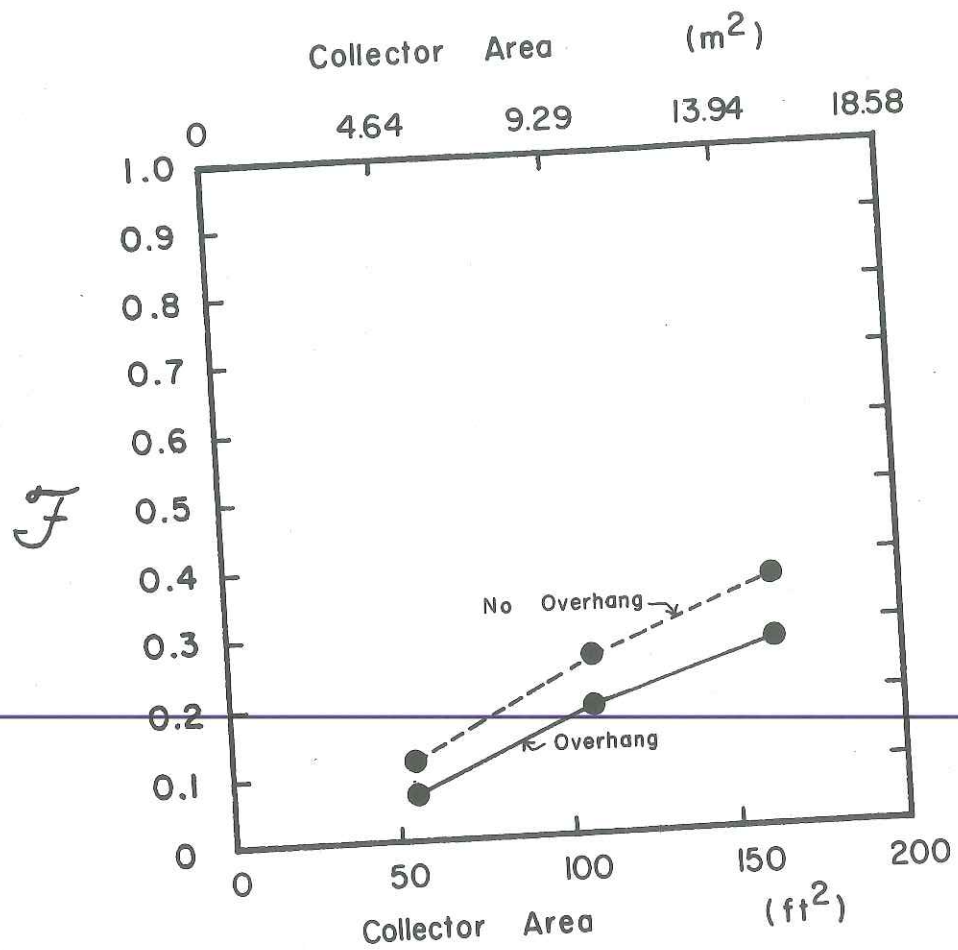
Figure 6.8 Effect of Overhang Shading on the Annual Solar Fraction - Madison, Wisconsin

Table 7.1

Base Direct Gain Parameters and Control
Strategy for Simulations

Parameter		Value	
		English	SI
Area	A	$161 \ ft^2$	$15 \ m^2$
Number of Panes	nc	2	2
Thickness - extinction coefficient product	KL	0.0524	0.0524
Refractive index	RI	1.526	1.526
Night insulation resistance	R_{NI}	$1.5 \ \frac{Hr \ ft \ ^{o}F}{Btu}$	$0.26 \ \frac{m^{o}C}{w}$
Overhang projection	P	4.92 ft	1.5 m
gap	g	1.64 ft	0.5 m
extensions	$e_L \ \& \ e_R$	6.56 ft	2.0 m
House Capacitance	C	$21060 \ \frac{Btu}{^{o}F}$	$40000 \ \frac{KJ}{^{o}C}$

Insulation is placed over the window at night
from November through April.

direct gain systems are compared to collector-storage walls and flat plate collector systems in the Madison climate.

7.2 Effect of Collector Area and Number of Window Panes

The annual solar fraction as a function of collector area for one, two and three window panes is plotted in Figure 7.1. Three panes are only marginally better than two panes, indicating that the higher solar transmittance of two panes is roughly balanced by the lower heat transfer coefficient of three panes. One pane exhibits a significantly lower performance.

All three plots show a definite nonlinear relationship between the solar fraction and the collector area. As the collector area increases, the average room temperature also increases. The effect is to increase the building load and reduce the useful solar gain. For the curve representing a single window, the additional in solar gain, by changing from 121 ft^2 (11.2 m^2) to 161 ft^2 (15 m^2), is nearly balanced by the increased building load. The result is an insignificant increase in the solar fraction.

7.3 Effect of the Building Capacitance

In this study, it is assumed that the building air
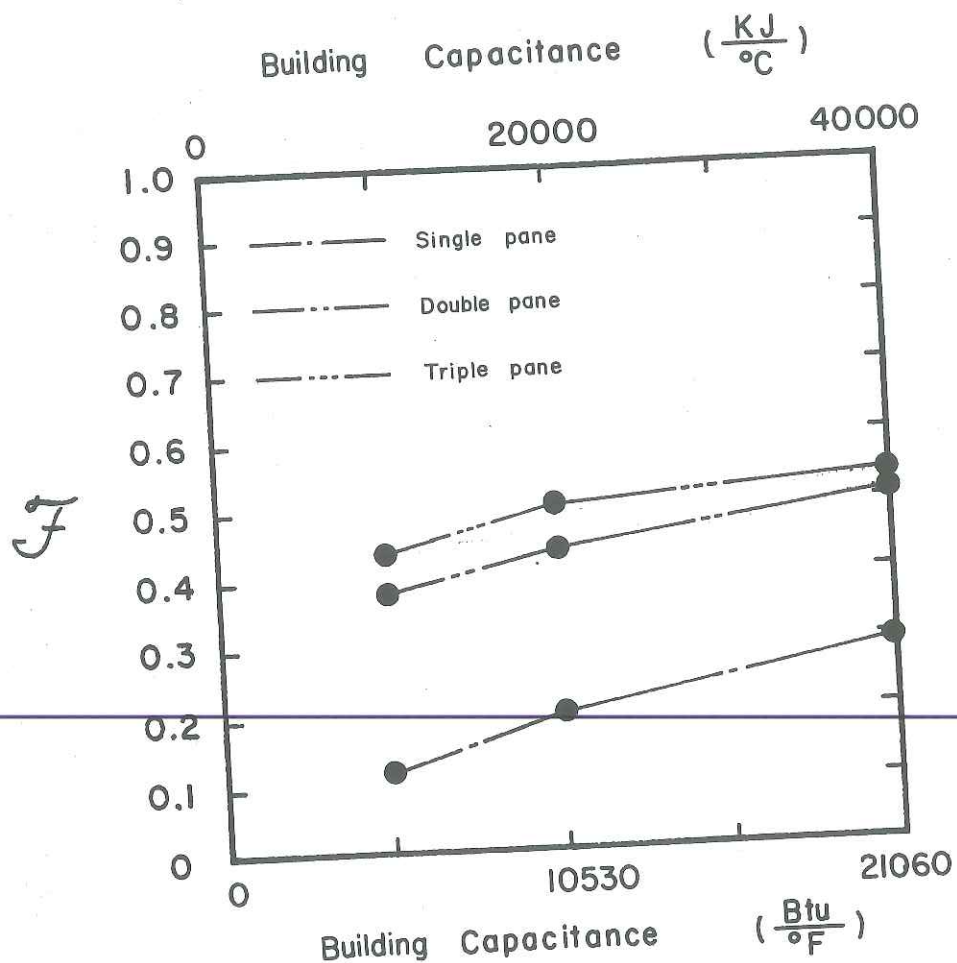
Figure 7.2 Effect of the Building Capacitance of a Direct Gain System on the Annual Solar Fraction - Madison, Wisconsin

both the building load and the energy vented to alleviate overheating are greater than the increased solar gain. This result suggests that there is an optimum window area for a given building capacitance. There is a difficulty, as stated above, in determining the appropriate building capacitance for a given situation. Only a fraction of a building's thermal mass is irradiated at any time of the day. The thermal storage and the windows must be located such that a large fraction of the desired thermal storage is irradiated by the sun throughout the day. Some existing solutions to this problem are worth mentioning.

MIT solar house V (T. Johnson (1978)) uses phase change materials encased in polymer concrete to increase the storage capabilities relative to the weight of the structure. The panels form the ceiling. Curved, reflecting louvers located between window panels reflect solar radiation onto the ceiling.

The Wallesey school, located in Liverpool, England, is a massive concrete structure with the exception of the south wall, which is all glass. The inner glass surface diffuses incoming solar radiation. This increases the level of solar radiation on the ceiling, back and side walls (M. G. Davies (1976)).
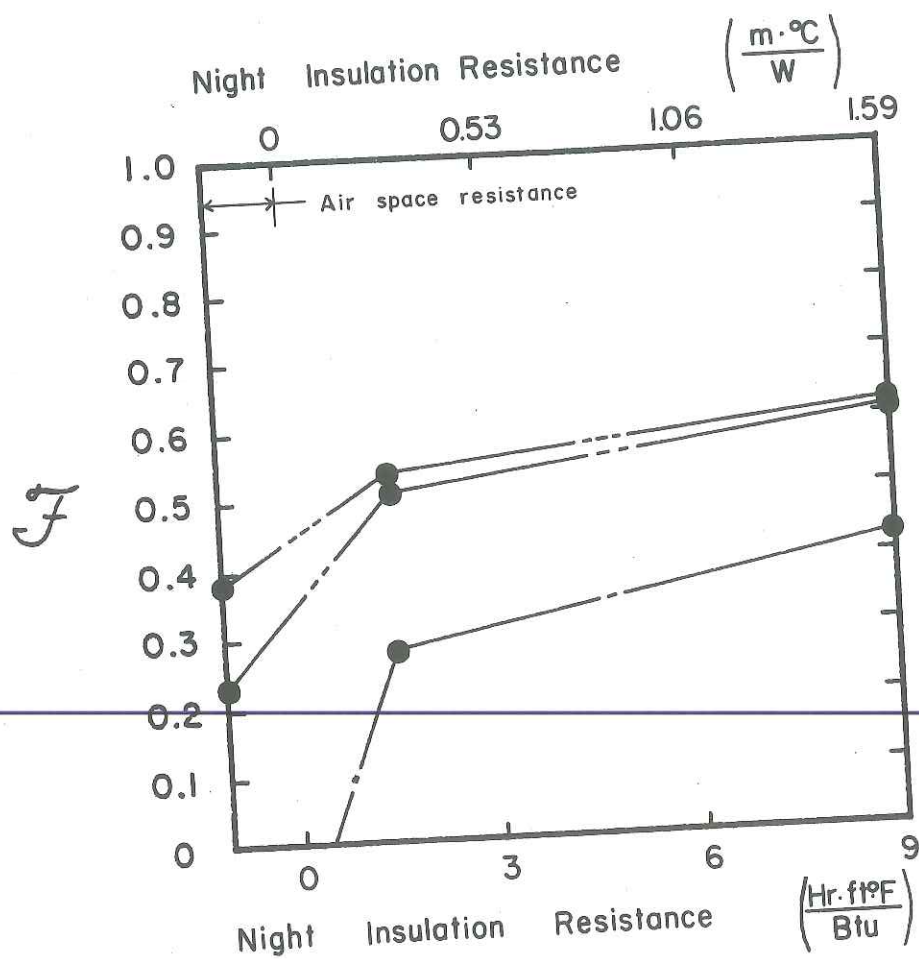
Figure 7.4 Effect of the Thermal Resistance of Night Insulation of a Direct Gain System on the Annual Solar Fraction - Madison, Wisconsin

ture is greater than 80°F (26.7°C) throughout the summer. Either adding an overhang or ventilating the building have nearly the same effect. Both strategies result in roughly 1800 hours of room temperature above 80°F (26.7°C) and a solar fraction of 0.6. However, using both over- hang and ventilation reduces the overheating hours to 409, near the 325 hours for base load 2 (see Table 5.3). With vent and overhang the solar fraction is only re- duced to 0.5. Both shading and ventilation are neces- sary to mitigate overheating. In Madison, the effect of each strategy is nearly equal. It has been assumed that a fan would be used to ventilate the building when overheating became a problem. With proper building de- sign, cross-flow ventilation driven by the wind can provide a significant portion of the required ventila- tion. Olgyay (1962) presents building design principles to enhance cross-flow ventilation, as well as simple tables to estimate the volume flow rate of the venti- lated air. No attempt is made in this study to assess the contribution of cross-flow ventilation.

7.6 Comparison of Direct Gain, Collector-Storage Wall and Flat Plate Collector Systems

A double pane, night insulated direct gain system, a triple glazed, 8 in (0.2 m) thick concrete collector-

storage wall, a single glazed, night insulated 12 in (0.3 m) water collector-storage wall and a double glazed flat plate water heating collector system are compared in Table 7.5. All systems have a 162 ft^2 (15 m^2) collector area and are connected to building load 2, described in Table 5.1. The direct gain system parameters are described in Table 7.1. The concrete collector-storage wall parameters are described in Table 6.2, except three covers are used instead of two. The water collector-storage wall parameters and control strategy are described in Table 7.3. The flat plate collector system is described in Table 7.4.

The annual solar fraction met by the flat plate collector system is determined using FCHART Version 3.0 solar heating design program developed by the Solar Energy Laboratory, University of Wisconsin-Madison. Monthly building energy loads for base load 2 (listed in Table 5.3) are used. The monthly meteorological data for Madison (summarized in Table 6.1) and the collector system parameters listed in Table 7.4 are input into the FCHART program which calculates the annual fraction of the heating base load supplied by solar energy. It is assumed that the required ventilation fan energy, Q_{FAN}, will remain unchanged with the addition of the flat plate collectors.

Table 7.4

Flat Plate Collector System Parameters
for Solar Heating Systems Comparison

Parameters	Value	
	English	SI
$F_R \ (\overline{\tau\alpha})$	0.7	0.7
$F_R \ U_L$	$0.83 \ \dfrac{Btu}{Hr \ ft^2 \ {}^oF}$	$4.72 \ \dfrac{w}{m^2 \ {}^o C}$
number of covers	2	2
collector slope	58°	58°
Storage capacity	$15 \ \dfrac{Btu}{{}^oF \ ft^2}$	$315 \ \dfrac{KJ}{{}^oC \ m^2}$

The annual solar fraction provided by the concrete collector-storage wall, 36%, is 22% less than the solar fraction provided by the water collector-storage wall. The increase in performance of the water wall is due (in order of importance) to the movable overhang, the use of one cover with night insulation instead of three covers, and the increased effective conductivity of the water wall. If the concrete wall had incorporated the same shading, night insulation and glazing strategies, a solar fraction of 53% could be expected. This figure is deter-mined by deducting 5% for the difference in performance due to conductivity and thickness from Figure 6.6. The conclusion is that the choice of shading and night insulating control strategies is more important than the choice of wall materials for the Madison climate.

The direct gain system gave a solar fraction of 0.51. Although the double pane window with a simple night in-sulating curtain is the least expensive solar collector of the four systems, the unknown costs and performance of the thermal storage make a discussion somewhat dif-ficult. The building thermal capacitance is 21060 $\frac{Btu}{°F}$ (40000 $\frac{KJ}{°C}$). By comparison, the water col-lector-storage wall (which can be thought of as a direct gain system with the thermal storage placed behind the window) has a total storage capacity of

energy gain of flat plate collectors. These results apply to Madison, Wisconsin. However, the winter climate in Madison is more severe than almost every major population center in the United States. As the winter climate becomes mild, the shading and night insulation control strategies become less important. When night insulation is not needed and a rigid overhang can be used, the cost-effectiveness of a collector-storage wall improves considerably.

One approach for harsh winter climates, which has not been well studied, is combining direct gain and flate plate collector systems. The Saskatchewan house, described by Besant and Dumont (1979) uses this approach coupled with a well insulated house (UA is 128 $\frac{Btu}{Hr\ ^{o}F}$ 68 $\frac{W}{^{o}C}$ with the insulated shutters closed). The total solar collection area includes 128 ft^2 (11.9 m^2) of south facing windows and 193 ft^2 (17.9 m^2) of evacuated tube solar collectors. The authors predict 100% of the space heating needs can be met by the solar heating system and internal gains in the 10800 ^{o}F-day (6000 ^{o}C-day) climate.

of f_i, the beam irriated fraction of the collection area, is then defined by five length parameters. However, since f_i is dimensionless, one length parameter can be used as a characteristic dimension and f_i can then be defined by four dimensionless length ratios. The characteristic dimension is the collector height. Division of the four remaining length parameters by the collector height gives the relative projection, $\tilde{p}$; the relative gap, $\tilde{g}$; the relative width, $\tilde{w}$; and the relative extension, $\tilde{e}$.

8.3 Long Term Average Solar Radiation on a Shaded Collector

The long term performance of a solar energy conversion system can be characterized by the monthly average daily solar radiation incident on the collector. By integrating equation [8.1] over a month and dividing the result by the number of days in the month, $\overline{H}_s$, the monthly average daily solar radiation per unit shaded collector area is obtained.

$$\overline{H}_s = \overline{H}_b \overline{R}_b \overline{f}_i + \overline{H}_d F_{c-s} + \frac{\rho}{2} \overline{H} \qquad [8.2]$$

$\overline{H}_b$, $\overline{H}_d$, and $\overline{H}$ are, respectively, the average daily beam, diffuse and total solar radiation on a unit horizontal surface. $\overline{R}_b$ is the total beam radiation on the collector

Equations [8.4] and [8.5] are compared in Table 8.1. Three locations, Albuquerque, New Mexico, Madison, Wisconsin and Seattle, Washington are considered. Weather data from each location is used to numerically evaluate equation [8.4]. The standard deviation between $\overline{F}_i$ determined by equation [8.4] and equation [8.5] for all locations is 0.012. The maximum difference is 0.04. The comparison is quite good, and equation [8.5] will be used to determine $\overline{F}_i$ in the following study.

Equation [8.2] requires $\overline{H}_b$, $\overline{H}_d$, and $\overline{H}$. Normally only $\overline{H}$ is known. Page (1961), Liu and Jordan (1960) and others have shown that the diffuse fraction of the average daily solar radiation, $\overline{H}_d/\overline{H}$, can be correlated to $\overline{K}_T$, the atmospheric clearness index. $\overline{K}_T$ is defined

$$\overline{K}_T = \frac{\overline{H}}{\overline{H}_o} \qquad [8.6]$$

$\overline{H}_o$ is the average daily extraterrestrial radiation on a unit horizontal surface. Rewriting equation [8.2] in terms of the diffuse fraction yields

$$\overline{H}_s = \overline{H} \left[(1 - \frac{\overline{H}_d}{\overline{H}}) \overline{R}_b \overline{F}_i + \frac{\overline{H}_d}{\overline{H}} F_{c-s} + \frac{\rho}{2} \right] \qquad [8.7]$$

Equation [8.7] provides an estimate of the monthly average daily solar radiation on a unit area of the shaded

collector. Values of $\overline{H}$ and $\overline{K}_T$ for many locations and correlations of $\overline{H}_d/\overline{H}$ are presented by Beckman, Klein, and Duffie (1977). The value of ρ varies from 0.2 to 0.7 depending on ground surface and snow cover. Values of F_{c-s}, the collector radiation view factor of the sky, are calculated from equation [2.11] and presented in Table 8.2 as a function of the four dimensionless geometry parameters. Values of $\overline{f}_i$ are presented below.

8.4 Values of $\overline{f}_i$

Values of $\overline{f}_i$, the average beam irradiated fraction of the collector area, have been calculated from equation [8.5] and plotted in Figures 8.1 through 8.9 as a function of the relative projection of the overhang. The collector is assumed to face due south. The figures include three northern latitudes (35°, 45°, and 55°) and three relative widths (1, 4 and 25). Each figure includes curves for three relative gaps (0., 0.2 and 0.4). The figures for relative widths of 1 and 4 include curves for two relative extensions (0. and 0.3). The mean monthly solar zenith angle decreases with increasing latitudes to yield a similar value of $\overline{f}_i$. Therefore, the length of the relative projection scale of the plots increases with latitude.
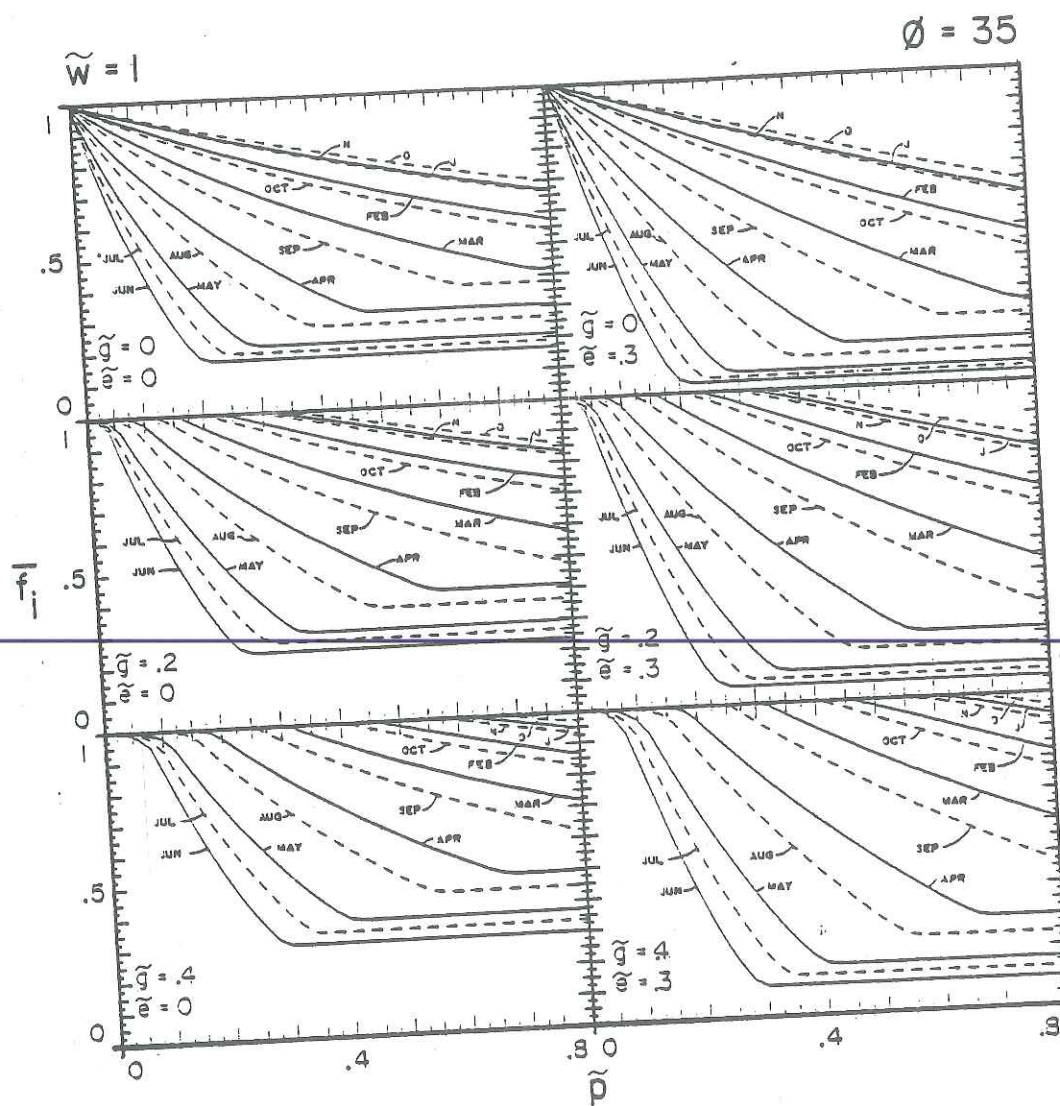
Figure 8.1 Plots of $\overline{F}_i$ for latitude of 35°N and relative width of 1
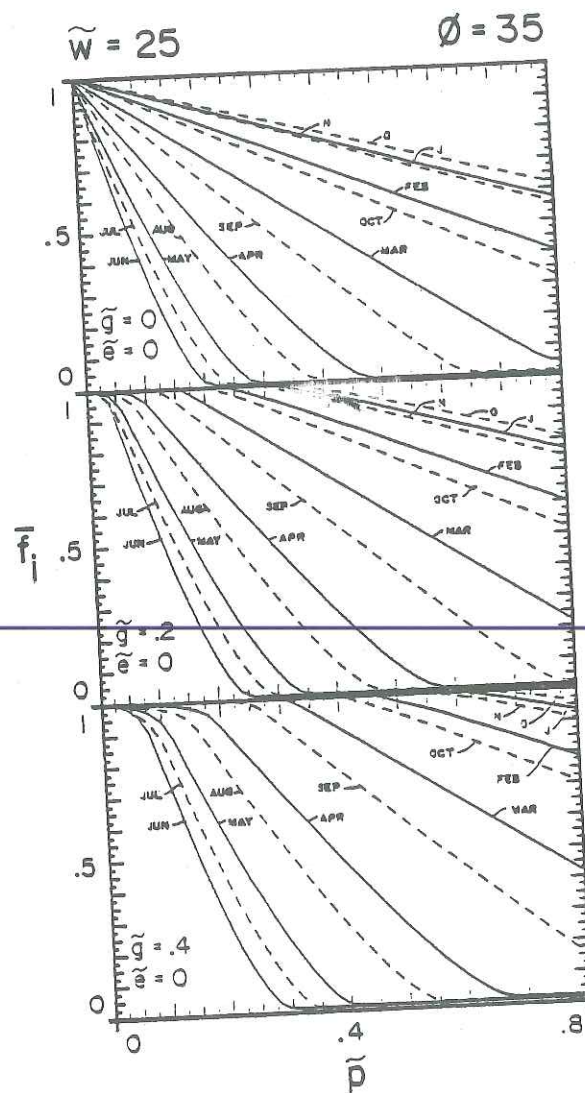
Figure 8.3 Plots of $\bar{F}_i$ for latitude of 35^ON and relative width of 25
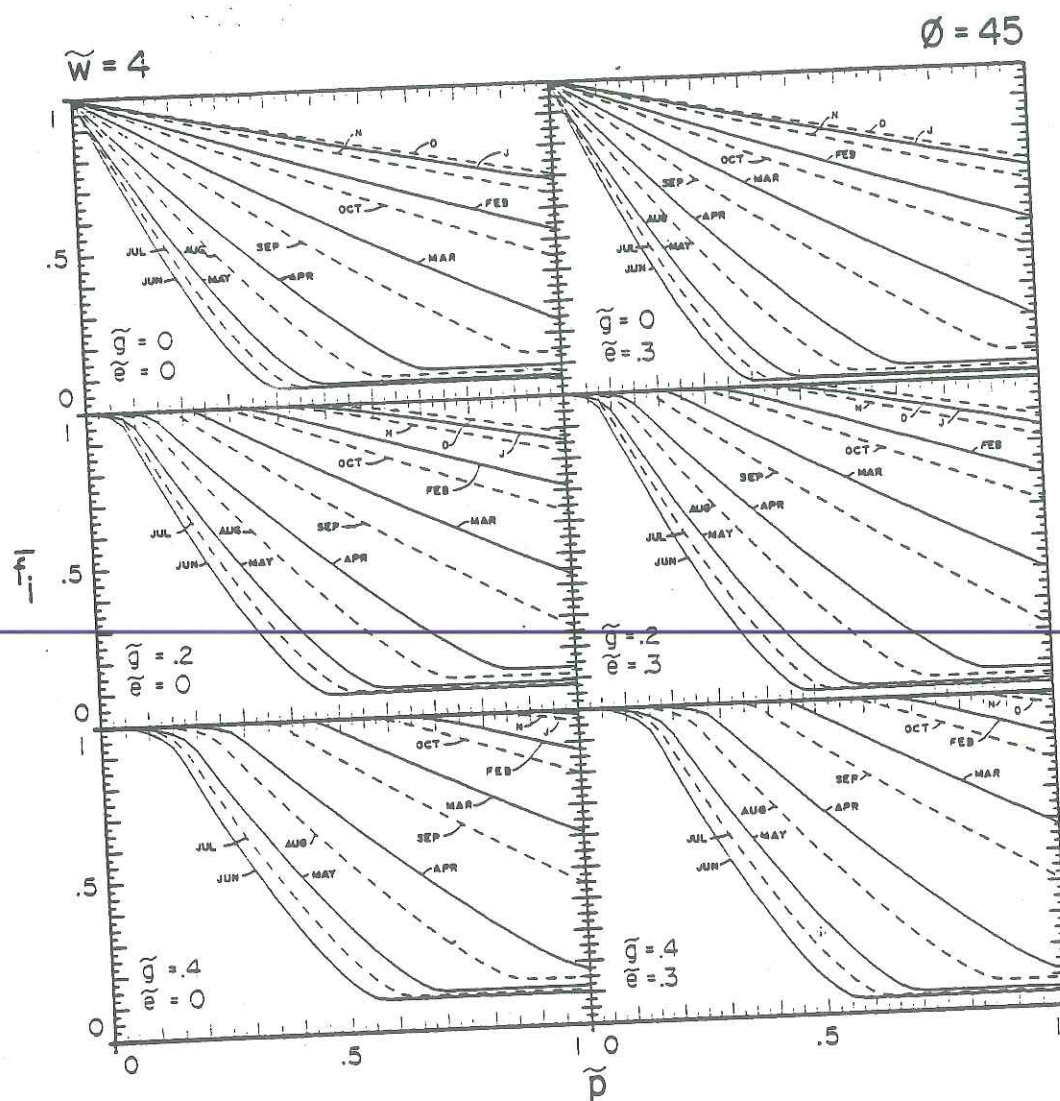
Figure 8.5 Plots of $\bar{f}_i$ for latitude of $45°N$ and relative width of 4
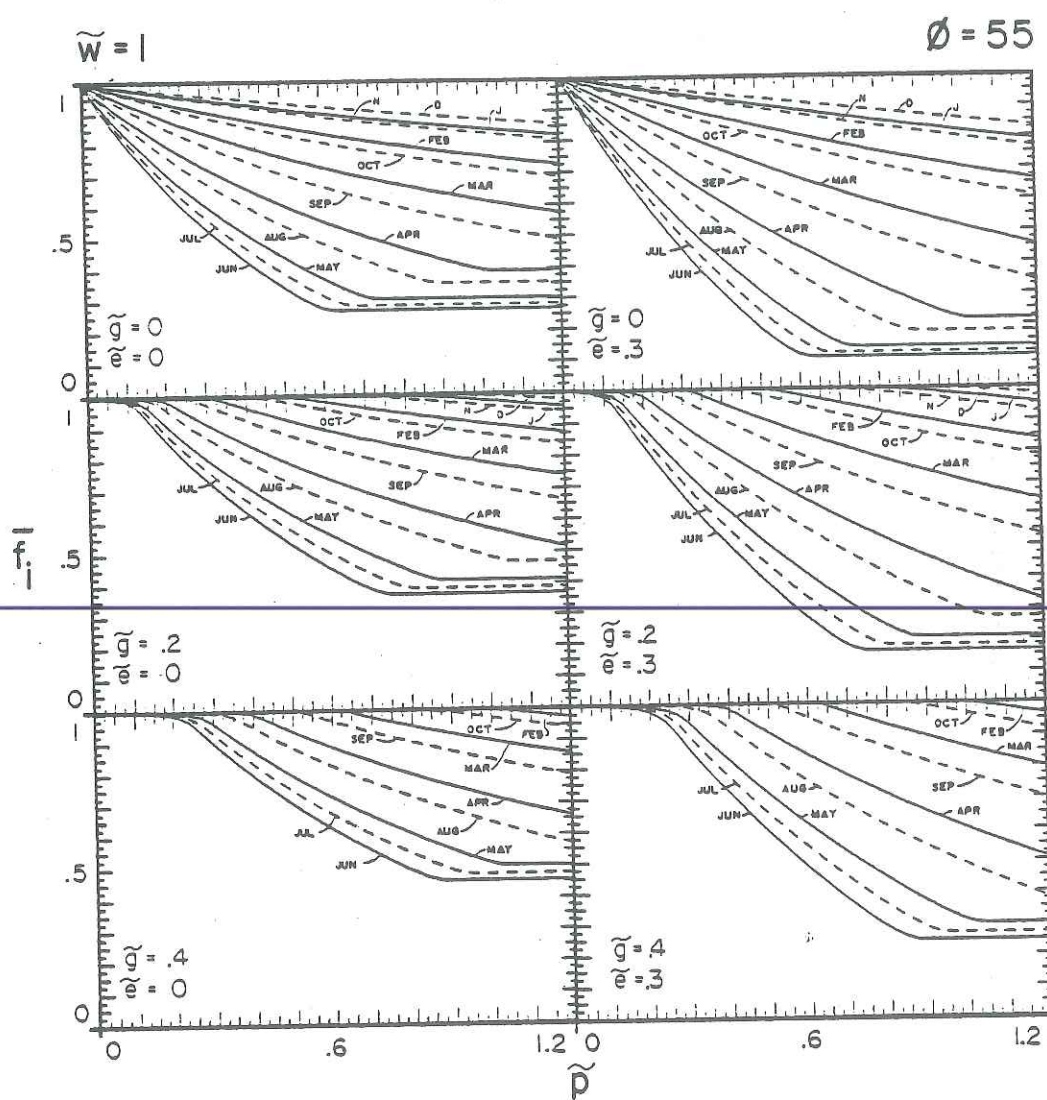
Figure 8.7 Plots of $\overline{f}_i$ for latitude of 55°N and relative width of 1
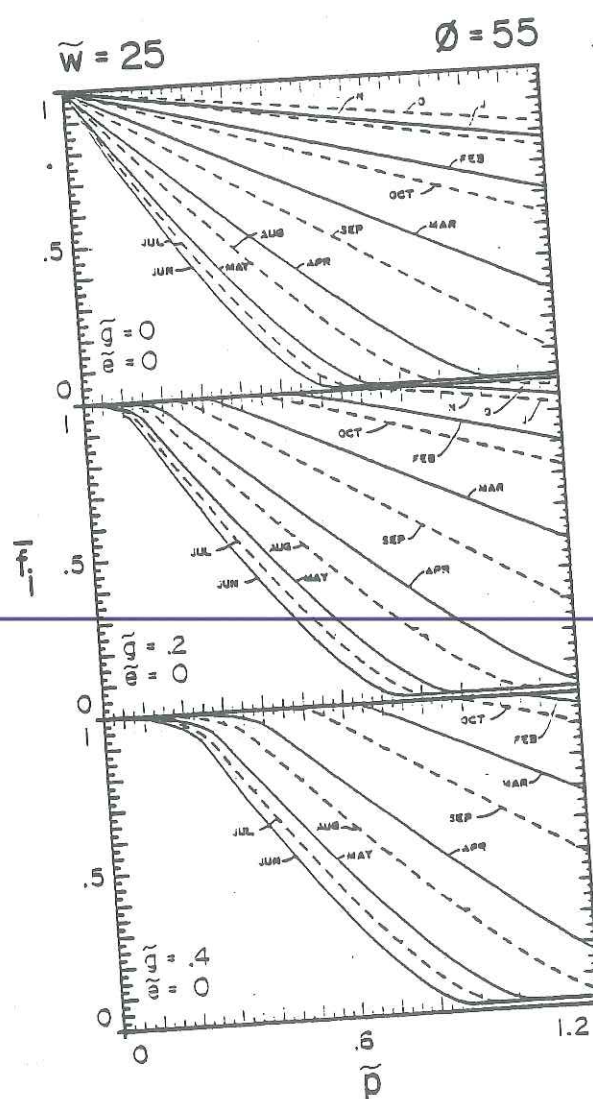
Figure 8.9 Plots of $\bar{f}_i$ for latitude of $55°N$ and relative width of 25

There are two features of the $\bar{F}_i$ curves that affect the interpolation process. First, the $\bar{F}_i$ curves have a limiting value of one during winter months and finite values of the relative gap. Second, the $\bar{F}_i$ curves cease to be a function of the relative projection during summer months at large relative projections. This behavior can be explained by reference to Figure 2.1. The shadow of the overhang on the collector surface is bounded by the horizontal shadow line of the edge of the projection and the diagonal shadow lines of the edge of the extensions. If the projection is large enough, the horizontal shadow line during a given month will always fall below the collector. Given this situation, $\bar{F}_i$ is not a function of the relative projection.

If $\bar{F}_i$ is not a function of the relative projection, then the interpolation of the correct value of $\bar{F}_i$ for a given relative gap must be between the two appropriate horizontal portions of the $\bar{F}_i$ curves. Thus, the value of the relative projection at which $\bar{F}_i$ ceases to be a function of the relative projection must be determined. For a given latitude and month, this value is a linear function of the relative gap. For example, for 45° north latitude and the month of June, $\bar{F}_i$ ceases to be a function of the relative projection at values of the relative

8.5   The Effect of the Extension on Values of $\overline{F}_i$

Published analyses of overhangs as shading devices have been based on the work of Olgyay and Olgyay (1957). These analyses assume the overhang extends infinitely past both sides of the collector. This assumption can seriously underpredict the beam radiation striking a shaded collector during the summer. The following analysis presents the conditions under which the infinite extension assumption can and cannot be applied.

The shadow of the edge of the extension forms a diagonal line on the plane of the collector. The location of the line relative to the collector is a function of time of day, latitude, extension and gap. If the extension is large, so that the extension shadow line never falls across the collector, the assumption of an infinite extension is valid. If the extension is small and the extension shadow line lies in the collector during the day, the value of $\overline{F}_i$ will increase due to beam radiation passing under the edge of the extension and striking the collector. The magnitude of the effect of the extension depends on the value of the relative width. Small relative widths intensify the effect of small extensions while very large relative widths completely damp out the effect of small extensions.
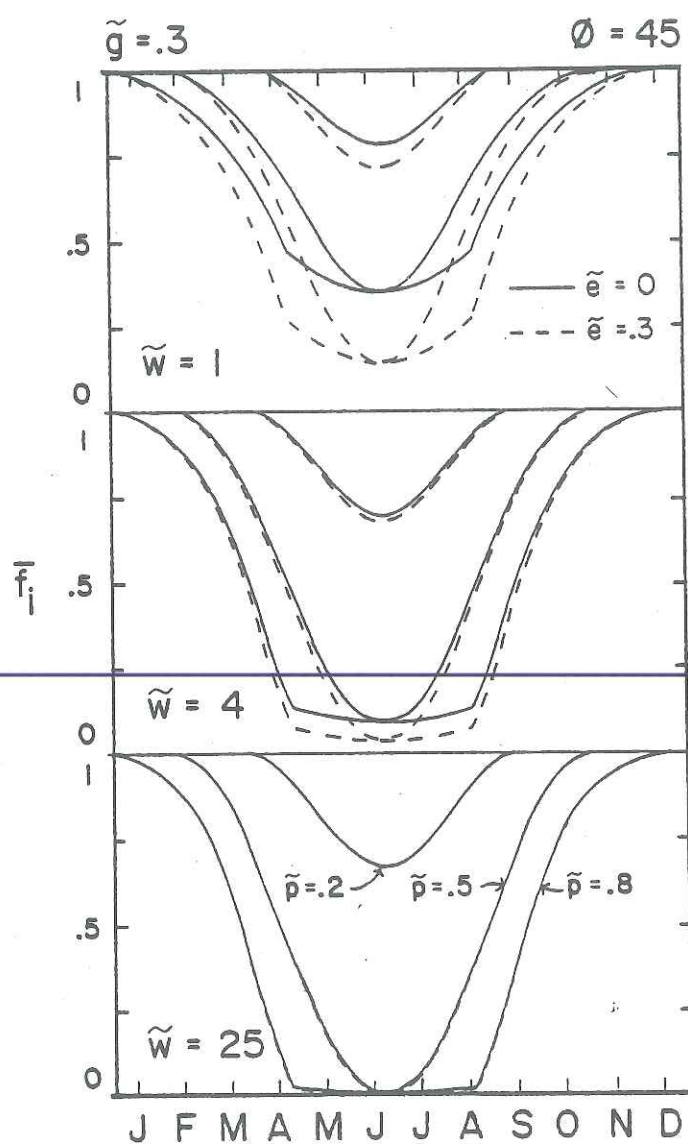
Figure 8.10   The effects of the relative extension and relative width on values of $\bar{f}_i$
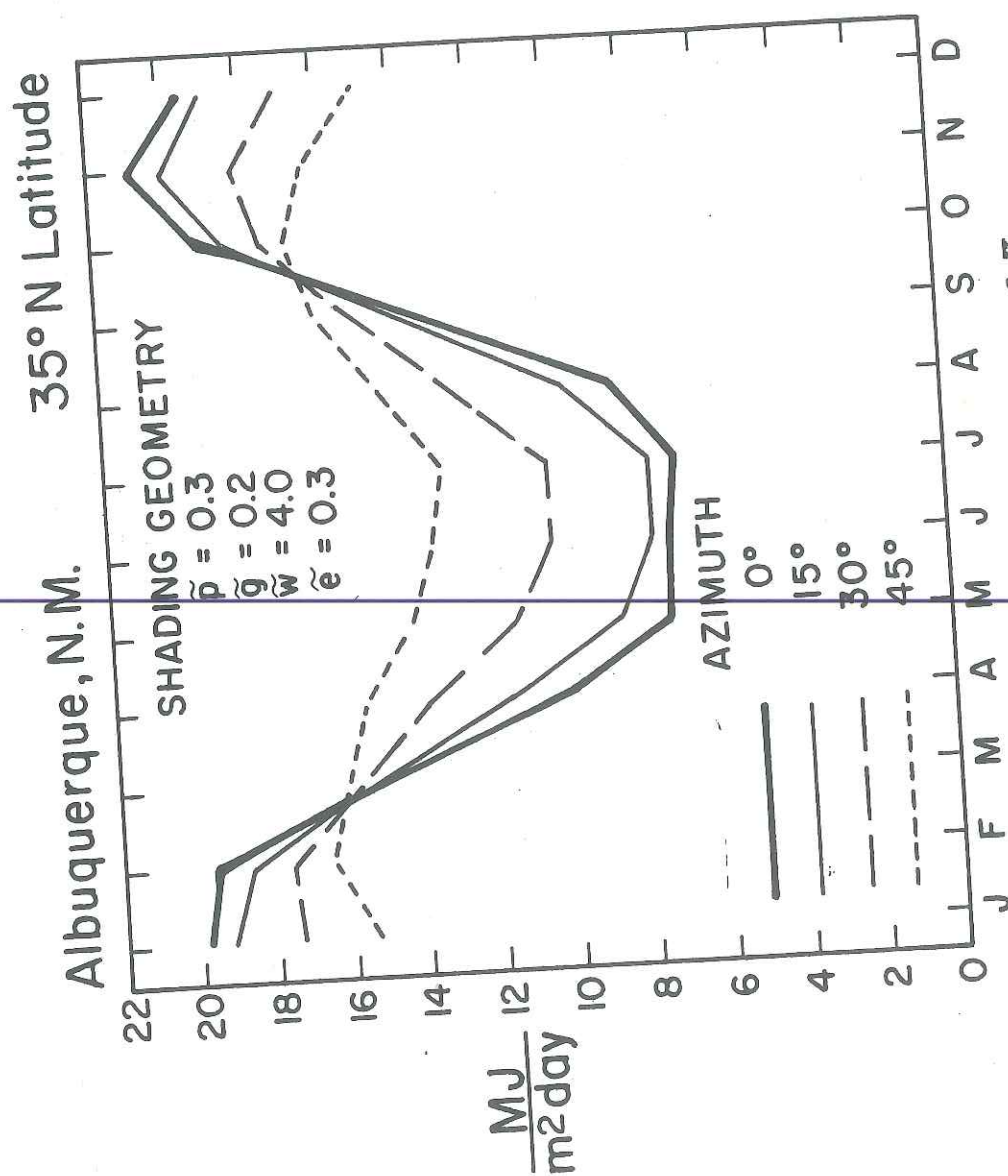
Figure 8.12 The effects of azimulth on values of H_s for receivers located in Albuquerque, NM

Table 8.3

Monthly Average Daily Solar Radiation on a Shaded Collector

Located in Madison, Wisconsin 43°N Latitude

Geometry p=0.5 g=0.25 e=0 $\tilde{w}$=6.0 F_{c-s}=0.40

	JAN	FEB	MAR	APR	MAY	JUN	JUL	AUG	SEP	OCT	NOV	DEC
$\bar{H}$ $\dfrac{Btu}{ft^2\,day}$ $\left[\dfrac{MJ}{m^2\,day}\right]$	5.61 (6.41)	8.12 (9.22)	12.30 (13.99)	14.60 (16.53)	17.40 (19.82)	20.30 (23.07)	20.50 (23.24)	17.40 (19.76)	14.40 (16.40)	9.93 (11.28)	5.56 (6.31)	4.96 (5.63)
$\bar{K}_T$	0.49	0.50	0.54	0.40	0.51	0.56	0.58	0.56	0.58	0.55	0.44	0.48
$\bar{H}_d/\bar{H}$	0.38	0.37	0.33	0.38	0.36	0.32	0.31	0.31	0.33	0.33	0.42	0.39
$\bar{R}_b$	2.68	1.80	1.07	0.55	0.30	0.21	0.25	0.43	0.83	1.52	2.41	3.00
	0.6	0.4	0.2	0.2	0.2	0.2	0.2	0.2	0.2	0.2	0.2	0.4
$\bar{F}_i$	0.99	0.93	0.79	0.46	0.16	0.05	0.09	0.32	0.67	0.90	0.98	0.99
$\bar{H}_s$ $\dfrac{Btu}{ft^2\,day}$ $\left[\dfrac{MJ}{m^2\,day}\right]$	12.00 (13.6)	11.50 (13.1)	9.77 (11.1)	5.95 (6.76)	4.68 (5.31)	4.81 (5.46)	4.78 (5.43)	5.61 (6.37)	8.89 (10.1)	11.40 (13.0)	9.16 (10.4)	10.80 (12.3)

Figure 8.13   Components of solar radiation striking a shaded receiver
in Minneapolis, MN

tor located in Albuquerque). Even though the summer value of $\bar{K}_T$ averaged 0.72 in Albuquerque compared to 0.53 in Minnesota, the overhang has a larger effect in reducing radiation in Minneapolis than in Albuquerque. This is partly due to differences in the average value of $\bar{R}_b$ during these three months (0.28 in Minneapolis and 0.14 in Albuquerque) and partly to using a value of the ground reflectance of 0.2 in Minneapolis and 0.3 in Albuquerque. In both locations the amount of radiation incident on the shaded collector during the summer is significant. It is evenly divided between diffuse and ground reflected radiation. The overhang does shade a significant amount of radiation from the collector during summer, although a larger amount of radiation remains unshaded.

8.9 Conclusions

An overhang is an effective device for shading a collector from direct beam radiation in the summer while leaving the collector unshaded in the winter. The total reduction of radiation on the collector in summer due to the shade can be less than 50% of the total radiation on an unshaded collector. The effect of collector azimuth on $\bar{H}_s$ is small when the azimuth is between 15° eash or west

CHAPTER 9

A SIMPLE NOMOGRAPH FOR SIZING OVERHANGS

9.1 Introduction

An overhang can be designed to shade a vertical, south facing solar collector totally during summer while leaving the collector unshaded during winter. Typically, the design process involves examination of the profile angle. The Sun Angle Calculators, developed by LOF (1951), can be used to evaluate the profile angle required to shade a collector during a specified period of the year. Using trigonometric formulas, (equations [9.5] and [9.6] below) the overhang can be sized. In this chapter a nomograph is described which gives the relative overhang projection and gap directly as a function of the latitude, number of days the collector is to be shaded and number of days the collector is to be unshaded.

9.2 The Profile Angle

The profile angle* is defined to be the angle between the plane of the collector and a plane containing the sun and passing through the horizontal edge of the

---

*The profile angle described with the Sun Angle Calculators is defined from the horizon, instead of the zenith. It is equal to $90° - \psi$.
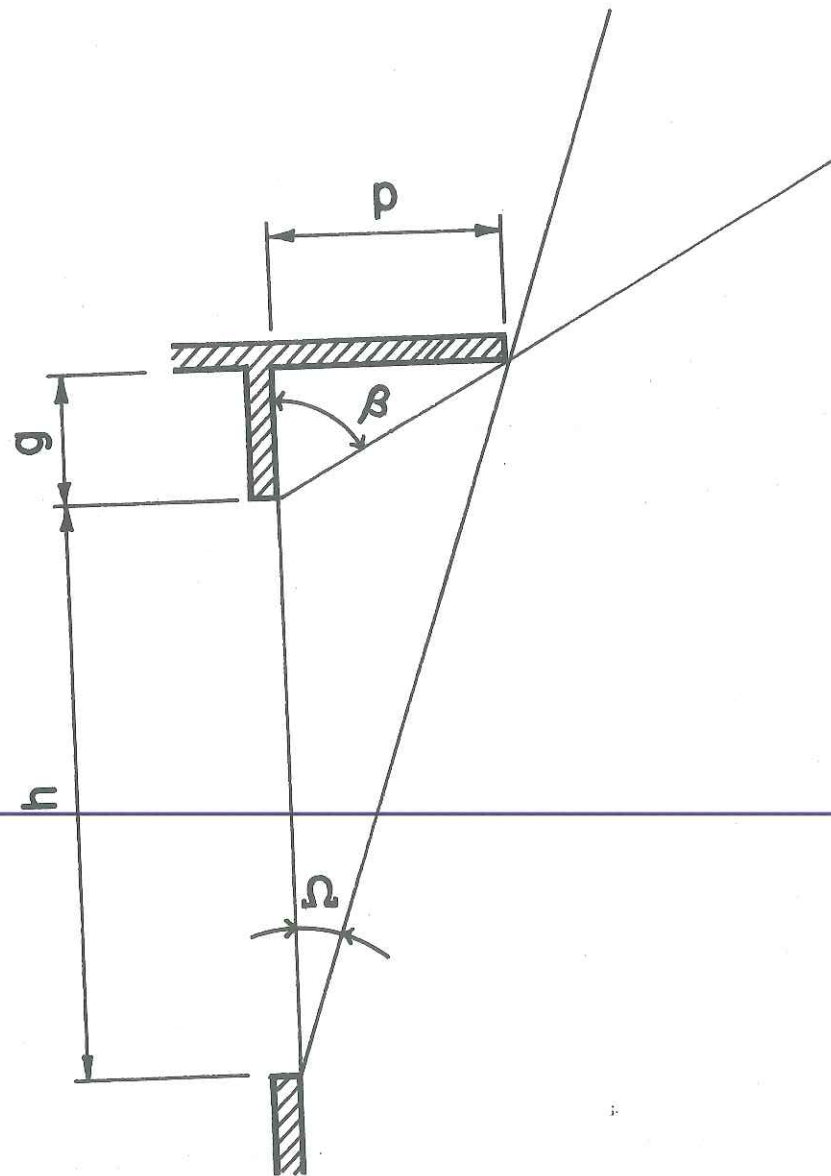
Figure 9.1   Angles and Dimensions Defining a Shaded and Unshaded Collector

9.3 The Nomograph and an Example of Its Use

The nomograph for the design of overhangs is shown in Figure 9.2. The relative projection, $\tilde{p}$ is found on the abcissa and the relative gap, $\tilde{g}$ on the ordinate. Four constant latitude curves and five constant declination curves are plotted on the nomograph. The declination curves are plotted by the number of days before and after the solstice that the collector is to be shaded or unshaded. For example, a collector located at 45° North latitude is to be totally shaded 30 days before and after the summer solstice and totally unshaded 30 days before and after the winter solstice. The point of intersection of the 45° latitude curve and the + 30 days curve is found and the values of p and g for the intersection point are read from the nomograph ($\tilde{p} = .57$ and $\tilde{g} = .26$). If the collector has a height of 10 ft (3.0 m), then a projection of 5.7 ft (1.74 m) and gap of 2.6 ft (0.79 m) would totally shade the collector 60 days during summer and leave the collector totally unshaded 60 days during winter.

Overhangs with unequal summer and winter shading can also be designed from the nomograph. The design of an overhang for Madison, Wisconsin ($\phi = 43^{\circ}$) will be used to illustrate the method. The collector is to be totally shaded 30 days before and after the summer solstice and

unshaded for 60 days before and after the winter solstice. The collector height is 6 ft (0.7 m). The solution is shown in Figure 9.3 and described here. First, the curve for 43° latitude is located by linear interpolation between the 35° and 45° curves. Next, a line is drawn from point B through the intersection of the 43° curve and $\pm$ 30 day curve. This line and the ordinate form the angle Ω. Next, a line is drawn from point T through the intersection of the 43° curve and the $\pm$ 60 days curve. This line and the ordinate form the angle β. The point of intersection of the two lines locates the edge of the overhang. $\tilde{p}$ and $\tilde{g}$ are, respectively, 0.58 and 0.41. For the 6 ft (0.7 m) high collector, the required projection is 3.48 ft (1.1 m) and the required gap is 2.46 ft (0.75 m). The nomograph will give accurate values of $\tilde{p}$ and $\tilde{g}$ if the vertical collector is south-facing and if the assumption of infinite overhang extensions is valid. Conditions for which the infinite extension can be assumed are described in section 8.5.

CHAPTER 10

SUMMARY AND DISCUSSION

10.1 Summary

Three building components, shading devices, windows and collector-storage walls, have been analyzed in relation to the direct solar heating of buildings. For each component, the following results are noted and conclusions drawn.

(A) Overhangs and Wingwalls

For south facing collectors, wingwalls are not effective as shading devices because they shade the collector during winter as well as during summer. When the collector faces toward the southeast or southwest, a single wingwall placed to the north of the collector can provide some shading during summer without shading the collector during winter.

Overhangs can shade south facing collectors totally during summer but not shade the collector at all during winter. Simulation studies for Madison, Wisconsin indicate that the overhang significantly reduces building overheating for both the direct gain and collector-storage wall systems. Furthermore, a moveable overhang, that only covers the collector from May through September,

the solar fraction when compared to the no flow condition. This result is in agreement with Ohanessian (1976) who examined a more mild climate. (iii) At low solar fractions, decreasing the thickness increases performance slightly. At high solar fractions, decreasing the thickness from 8 in (0.2 m) to 4 in (0.1 m) significantly reduces the performance. Increasing the thermal capacitance does not significantly affect performance. For thick walls, increasing the conductivity significantly increases performance.

(c)   Direct Gain Systems

Direct gain systems were coupled to the same building load as the collector-storage wall and simulated in Madison, Wisconsin to study the effects of the design parameters. The following results were obtained. (i) Insulating the window at night significantly increased the solar fraction (even though the thermal resistance of the curtain and air space was only 2.6 Hr ft^2 °F/Btu (0.46 m^2°C/w). With night insulation, the solar fraction was nearly identical for 2 or 3 window panes but significantly lower for 1 window pane. (ii) While increasing the building thermal capacitance increased the solar fraction, uncertainties concerning the actual thermal capacity and response of direct gain

questionable because of uncertainties concerning lumped capacitance assumptions. The relationship between large solar gains and building thermal response needs to be studied in detail. However, rules of thumb regarding building design practice during the 1950's recommended 25% to 40% of the south facade could be window. The construction did not need to be modified to increase thermal mass. Add to this rule of thumb the application of night insulation and the windows become very effective solar collectors (in terms of both cost and thermal performance). This strategy has often been called sun-tempered architecture. While it certainly represents sound architectural practice, one need only examine the buildings constructed today to see how rarely the strategy is used.

A method of estimating solar radiation on vertical south facing collectors is presented. Although the method applies to overhangs with finite extensions, it is somewhat cumbersome, since it requires graphic interpolation. If the infinite overhang extension is valid, then the analytical method of estimating radiation on shaded collectors that is presented by Jones (1979) should be used. The nomograph to size overhangs that is presented in this study should be helpful to architects since it is simple and quick.

consuming buildings (compared to townhouses and apart-
ments) and energy consuming transportation habits. It
is hoped that the American dream can be reformulated
in an energy conserving direction. In this direction,
solar heating can and would play a major role in reducing
our energy consumption.

Table A.1

Results of Simulations Presented in Chapter 6

Values presented in Giga Joules, to convert to MMBtu multiply the number in the table by 0.9478

Figure 6.1

base load	A m²	Q_L	Q_{VNT}	Q_b	*Q_v	Q_{in}	Q_{AUX}	Q_{FAN}	Q_{PAR}	Q_{TOT}	number of hours $T_b > 80°F$ (26.7°C)
1	5	36.6	1.4	1.39	0.87	2.26	35.8	0.7	0	36.5	198
1	10	35.8	1.7	3.02	1.29	5.31	33.2	0.8	0	34.0	234
1	15	35.1	1.9	4.66	1.61	6.27	30.8	0.8	0	31.6	282
2	5	18.4	1.2	1.40	0.86	2.26	17.4	0.6	0	18.0	62
2	10	17.7	1.5	2.98	1.25	4.23	15.0	0.7	0	15.7	107
2	15	17.0	2.0	4.50	1.51	6.01	13.0	0.9	0	13.9	189

Figure 6.2

nc	A m²	Q_L	Q_{VNT}	Q_b	*Q_v	Q_{in}	Q_{AUX}	Q_{FAN}	Q_{PAR}	Q_{TOT}	number of hours $T_b > 80°F$ (26.7°C)
1	5	18.4	1.2	0.81	0.37	1.18	18.5	0.6	0	19.1	64
1	10	17.6	1.5	1.58	0.51	2.09	17.1	0.7	0	17.8	119

*Q_v includes energy vented to the house only.

Table A.1 (continued)

x m	k w/m°C	ρ KJ/m³°C	Q_L	Q_{VNT}	Q_b	Q_v	Q_{in}	Q_{AUX}	Q_{FAN}	Q_{PAR}	Q_{TOT}	number of hours $T_b > 80°F$ (26.7°C)
3	(0.26)		17.1	2.0	6.78	2.76	9.54	9.6	0.8	0	10.4	180
1	∞		17.2	2.2	7.31	2.28	9.59	9.8	0.9	0	10.7	242
2	∞		17.4	2.2	8.20	3.45	11.65	8.0	0.9	0	8.9	235
3	∞		17.4	2.1	8.04	3.91	11.95	7.5	0.9	0	8.4	199
0.4	6.92	4000	17.6	2.7	10.07	0	10.07	10.3	1.8	0	12.1	361
0.4	6.92	2000	17.8	2.8	9.94	0	9.94	10.6	1.8	0	12.4	470
0.4	1.73	4000	17.3	2.0	7.76	0	7.76	11.5	1.7	0	13.2	296
0.4	1.73	2000	17.4	2.1	7.82	0	7.82	11.7	1.7	0	13.4	343
0.4	0.43	4000	16.7	1.2	4.15	0	4.15	13.7	1.4	0	15.1	187
0.4	0.43	2000	16.7	1.2	4.07	0	4.07	13.9	1.4	0	15.3	223
0.25	6.92	4000	17.8	2.8	10.28	0	10.28	10.4	1.8	0	12.2	454

Figure 6.6

Table A.1 (continued)

	Thermocirculation		Q_L	Q_{VNT}	Q_b	Q_v	Q_{in}	Q_{AUX}	Q_{FAN}	Q_{PAR}	Q_{TOT}	number of hours $T_b > 80°F$ (26.7°C)
	no	no	17.1	2.4	5.75	1.00	6.75	12.7	1.0	0	13.7	238
25	no	no	17.2	2.4	4.87	2.00	6.87	12.8	1.0	0	13.8	208
25	yes	no	17.2	2.4	4.87	2.00	6.87	12.8	1.0	0.3	14.1	208
25	yes	yes	17.2	2.4	4.87	2.00	6.87	12.8	1.0	1.2	15.0	208
50	no	no	17.1	2.4	4.22	2.58	6.80	12.7	0.9	0	1.36	201
50	yes	no	17.1	2.4	4.22	2.58	6.80	12.7	0.9	0.5	14.1	201
50	yes	yes	17.1	2.4	4.22	2.58	6.80	12.7	0.9	1.7	15.3	201
100	no	no	17.1	2.2	3.10	3.45	6.55	12.8	0.9	0	13.7	178
100	yes	no	17.1	2.2	3.10	3.45	6.55	12.8	0.9	0.8	14.5	178
100	yes	yes	17.1	2.2	3.10	3.45	6.55	12.8	0.9	2.8	16.5	178

Figure 6.8

Overhang	A m²	Q_L	Q_{VNT}	Q_b	Q_v	Q_{in}	Q_{AUX}	Q_{FAN}	Q_{PAR}	Q_{TOT}	number of hours $T_b > 80°F$ (26.7°C)
no	5	18.8	1.6	2.93	1.16	4.09	16.4	0.8	0	17.2	165
no	10	18.6	2.8	6.47	1.74	8.21	13.3	1.1	0	14.4	446

Table A.2

Results of Simulations Presented in Chapter 7

Figure 7.1

nc	A_m^2	Q_L	Q_{VNT}	Q_{in}	Q_{AUX}	Q_{FAN}	Q_{TOT}	number of hours $T_b > 80°F$ (26.7°C)
1	7.5	18.7	2.2	5.9	15.1	0.9	16.0	29
1	11.25	18.6	3.3	9.3	12.8	1.2	14.0	230
1	15	18.1	4.0	9.7	12.5	1.3	13.8	417
2	7.5	18.7	2.2	8.2	12.8	0.9	13.7	11
2	11.25	18.7	3.5	12.8	9.6	1.2	10.8	172
2	15	18.4	4.4	14.8	8.2	1.4	9.6	409
3	7.5	18.6	2.0	8.2	12.6	0.9	13.5	4
3	11.25	18.6	3.3	12.8	9.2	1.2	10.4	105
3	15	18.3	4.1	15.1	7.5	1.4	8.9	309

Table A.2 (continued)

			Q_L	Q_{VNT}	Q_{in}	Q_{AUX}	Q_{FAN}	Q_{TOT}	number of hours $T_b > 80°F$ (26.7°C)
2	11.25	10000	19.4	4.3	12.5	11.3	1.4	12.7	672
3	11.25	10000	19.2	3.8	12.6	10.5	1.3	11.8	558

All other points given in listings of Figure 7.1 and Figure 7.2 above

Figure 7.4

nc	$R_{NI} \frac{m^2 °C}{W}$	Q_L	Q_{VNT}	Q_{in}	Q_{AUX}	Q_{FAN}	Q_{TOT}	number of hours $T_b > 80°F$ (26.7°C)
1	0	17.9	3.7	-3.6	25.4	1.3	26.7	398
1	0.26	Figure 7.1 above (A = 15 m² & nc = 1)						
1	1.59	18.4	4.0	12.9	9.8	1.3	11.1	450
2	0	18.2	4.2	9.1	13.5	1.4	14.9	414
2	0.26	Figure 7.1 above (A = 15 m² & nc = 2)						
2	1.59	18.6	4.5	17.2	6.1	1.5	7.6	431
3	0	18.1	4.0	11.9	10.4	1.4	11.8	322
3	0.26	Figure 7.1 above (A = 15 m² & nc = 3)						
3	1.59	18.4	4.2	16.9	5.9	1.4	7.3	307

Johnson, T.E. "Preliminary Performance of the MIT Solar Building V," Proceedings of the 2nd National Passive Solar Conference, Philadelphia, PA, pp. 610-616, March 16-18, (1978).

Jones, R.E. "Effects of Overhang Shading of Windows Having Arbitrary Azimuth," to be published in Solar Energy.

Klein, S.A. "Calculation of Collector Loss Coefficients," Solar Energy, vol. 17, (1975) pp. 79-80.

Klein, S.A. "Calculation of Monthly Average Insolation on Tilted Surfaces," Solar Energy, vol. 19, no. 4, (1977) pp. 325-329.

Libby-Owens-Ford Glass Company. "The Sun Angle Calculator," Copyright (1951).

Liu, B.Y.H. and Jordan, R.C. "Daily Insolation of Surfaces Tilted Toward the Equator," Trans. ASHRAE, 526 (1962).

Liu, B.Y.H. and Jordan, R.C. "The Interrelationship and Characteristic Distribution of Direct, Diffuse and Total Solar Radiation," Solar Energy, vol. 4, no. 3, (1960).

McAdams, W.C. Heat Transmission, 3rd ed, New York, McGraw-Hill, (1954).

McFarland, R.D., and Balcomb, J.D. "Effects of Design Parameter Changes on the Performance of Thermal Storage Wall Passive Systems," Proceedings of the 3rd National Passive Solar Conference, San Jose, CA, pp. 54-60, Jan. 11-13, (1979).

Mercer, W.E., Pearce, W.M., and Hitchcock, J.E. "Laminar Forced Convection in the Entrance Region Between Parallel Flat Plates," J. of Heat Transfer, vol. 89, (1967), pp. 251-257.

Ohanessian, P. "Numerical Modelling of a Passive Solar Energy House Heating System," M.S. thesis, University of Melbourne, (1976).

Ohanessian, P., and Charters, W.W.S. "Thermal Simulation of a Passive Solar House Using a Trombe-Michel Wall Struvture," Solar Energy, vol. 20, no. 3, (1978), pp. 275-281.